H3.1K27me1 maintains transcriptional silencing and genome stability by preventing GCN5-mediated histone acetylation

RESEARCH ARTICLE

H3.1K27me1 maintains transcriptional silencing and genome stability by preventing GCN5-mediated histone acetylation

Jie Dong[1,2,#], Chantal LeBlanc[1#], Axel Poulet[1#], Benoit Mermaz[1], Gonzalo Villarino[1], Kimberly M. Webb[3], Valentin Joly[1], Josefina Mendez[1], Philipp Voigt[3], and Yannick Jacob[1*]

[1] Yale University, Department of Molecular, Cellular and Developmental Biology, Faculty of Arts and Sciences; 260 Whitney Avenue, New Haven, Connecticut 06511, United States.
[2] Current address: Institute of Crop Science, Zhejiang University, Hangzhou 310058, China.
[3] Wellcome Centre for Cell Biology, School of Biological Sciences, University of Edinburgh, Edinburgh EH9 3BF, United Kingdom.
# These authors contributed equally to this manuscript.
* Corresponding author: yannick.jacob@yale.edu

Short title: H3K27me1 antagonizes GCN5 in heterochromatin

One-sentence summary: The histone post-translational modification H3.1K27me1 maintains transcriptional silencing and genome stability by preventing histone acetylation mediated by the histone acetyltransferase GCN5.

The author responsible for distribution of materials integral to the findings presented in this article in accordance with the policy described in the Instructions for Authors (www.plantcell.org) is: Yannick Jacob (yannick.jacob@yale.edu).

Abstract

Epigenetic mechanisms play diverse roles in the regulation of genome stability in eukaryotes. In *Arabidopsis thaliana*, genome stability is maintained during DNA replication by the H3.1K27 methyltransferases ARABIDOPSIS TRITHORAX-RELATED PROTEIN 5 (ATXR5) and ATXR6, which catalyze the deposition of K27me1 on replication-dependent H3.1 variants. Loss of H3.1K27me1 in *atxr5 atxr6* double mutants leads to heterochromatin defects, including transcriptional de-repression and genomic instability, but the molecular mechanisms involved remain largely unknown. In this study, we identified the transcriptional co-activator and conserved histone acetyltransferase GCN5 as a mediator of transcriptional de-repression and genomic instability in the absence of H3.1K27me1. GCN5 is part of a SAGA-like complex in plants that requires the GCN5-interacting protein ADA2b and the chromatin remodeler CHR6 to mediate the heterochromatic defects in *atxr5 atxr6* mutants. Our results also indicate that Arabidopsis GCN5 acetylates multiple lysine residues on H3.1 variants, but H3.1K27 and H3.1K36 play essential functions in inducing genomic instability in the absence of H3.1K27me1. Finally, we show that H3.1K36 acetylation by GCN5 is negatively regulated by H3.1K27me1 *in vitro*. Overall, this work reveals a key molecular role for H3.1K27me1 in maintaining transcriptional silencing and genome stability in heterochromatin by restricting GCN5-mediated histone acetylation in plants.

Introduction

Genome and epigenome instability have been implicated in many human diseases, including cancer and neurodegenerative disorders. In proliferating cells, key mechanisms are required to properly copy DNA and different epigenetic states of the genome in the context of ongoing transcription and DNA repair. Chromatin replication is therefore a complex molecular operation that can lead to genomic rearrangements and other types of deleterious mutations in the absence of mechanisms preserving genome stability (Chen et al., 2010; Weinert et al., 2009).

Epigenetic information plays multiple regulatory roles during S phase of the cell cycle that are required to maintain genome stability in eukaryotes. In plants, one of the most well-studied genome maintenance pathways involves the histone post-translational modification (PTM) H3K27me1. The loss of H3K27me1 results in transcriptional de-repression at heterochromatic loci and defects in the structural organization of heterochromatin (Jacob et al., 2009; Stroud et al., 2012). In addition, decreased levels of H3K27me1 induce genome instability characterized by the presence of an excess of repetitive DNA (e.g. transposons) in heterochromatin, hereafter referred to as heterochromatin amplification (Jacob et al., 2010). In *Arabidopsis thaliana*, H3K27me1 is catalyzed by the plant-specific histone methyltransferases ATXR5 and ATXR6 (abbreviated ATXR5/6 hereafter), which are recruited to replication forks during DNA replication (Davarinejad et al., 2019; Jacob et al., 2009; Raynaud et al., 2006). Biochemical and structural studies have revealed that the SET domains of ATXR5/6 can methylate replication-dependent H3.1 variants, but not replication-independent H3.3 variants (Jacob et al., 2014). These observations indicate that ATXR5/6 maintain H3K27me1 by methylating newly synthesized H3.1 variants (H3.1K27me1) during DNA replication, which protects against transcriptional de-repression and heterochromatin amplification. The precise molecular mechanism responsible for heterochromatin amplification in the absence of H3.1K27me1 remains unknown. However, a previous study suggested that transcriptional de-repression in the heterochromatin of *atxr5 atxr6* double mutant plants (hereafter *atxr5/6*) is the cause of the genomic instability phenotype, potentially by inducing collisions between the transcription machinery and replication forks, and/or through R-loop formation (Hale et al., 2016). Based on this model, it is predicted that ATXR5/6-catalyzed H3.1K27me1 plays a key role in preventing transcriptional activity in the heterochromatin of plants.

Many PTMs on histones function as recruitment signals for chromatin reader proteins, which promote specific cellular activities (such as transcription) at genomic regions enriched in these histone PTMs (Musselman et al., 2012). Multiple studies have shown that methylation at H3K27 regulates transcriptional activity through various mechanisms, which are related to the specific methylation level (i.e., me1, me2 or me3) at K27. For example, H3K27me3 is involved in the recruitment of the repressive PRC1 complex in animals (Fischle et al., 2003), and this role is conserved in plants (Huang et al., 2019). H3K27me3 is also directly recognized by the PRC2 complex, which catalyzes K27me3 on histone H3, thus allowing for a "read-write" propagation mechanism that contributes to maintaining H3K27me3 levels *in vivo* (Hansen et al., 2008; Margueron et al., 2009; Xu et al., 2010). In contrast to H3K27me3, H3K27me1 and H3K27me2 are not as well characterized in animals, but they have specific effects on the regulation of transcriptional activity that do not appear to involve recruitment of chromatin readers. In mouse embryonic stem cells (ESCs), H3K27me2 is present on the majority of total histone H3 in chromatin and safeguards against unintended transcription by preventing CBP/p300-mediated H3K27 acetylation (H3K27ac) at non-cell-type-specific enhancers (Ferrari et al., 2014). By contrast, H3K27me1 is present at less than 5% of total H3s in ESCs, is associated with transcriptionally active genes, and contributes to their expression (Ferrari et al., 2014). However, the mechanism by which H3K27me1 performs this function remains unknown. Predicting the role of ATXR5/6-catalyzed H3K27me1 in plants based on comparative analysis with H3K27me1/me2 in animals is challenging, as it shares the same methylation level of transcriptionally permissive H3K27me1, but its function in heterochromatin silencing in plants suggests properties related to H3K27me2. An additional similarity between plant H3K27me1 and animal H3K27me2 is that these histone PTMs are widely distributed and very abundant in their respective genomes. In Arabidopsis, H3K27me1 was estimated to be present on more than 50% of total H3 in inflorescence tissues (Johnson et al., 2004), and it is enriched in transcriptionally silent regions of the genome (Jacob et al., 2010). These observations suggest that H3.1K27me1 in plants prevents H3.1K27ac, thus providing a molecular mechanism for the role of ATXR5/6 in protecting against transcriptional de-repression and genomic instability in plants.

In this work, we identify the conserved histone acetyltransferase GCN5 as a mediator of transcriptional de-repression and heterochromatin amplification in the absence of H3.1K27me1 in

Arabidopsis. GCN5 cooperates with the transcriptional co-activator ADA2b and the chromatin remodeler CHR6 to induce these heterochromatic phenotypes. Our results also show that H3.1K36 plays a key role in inducing genome instability and transcriptional de-repression in the absence of H3.1K27me1, and that H3.1K27me1 interferes with GCN5-mediated acetylation at both H3.1K27 and H3.1K36. Overall, these results demonstrate the key role played by GCN5-mediated histone acetylation in contributing to the heterochromatin phenotypes observed in the absence of ATXR5 and ATXR6 in plants.

Results

Transcriptional de-repression and heterochromatin amplification in the absence of H3.1K27me1 are suppressed in *gcn5* mutants

One mechanism by which H3.1K27me1 might interfere with transcription in heterochromatin of plants is by preventing the deposition of H3.1K27ac, as methylation and acetylation at H3K27 have been shown to act antagonistically in other biological systems (Pasini et al., 2010; Tie et al., 2009). H3K27ac is catalyzed by multiple histone acetyltransferases in eukaryotes, including the widely conserved protein GCN5 (Chen et al., 2017; Cieniewicz et al., 2014; Kuo et al., 1996; Kuo and Andrews, 2013; Suka et al., 2001). The Arabidopsis genome contains a single gene encoding a GCN5 homolog (Pandey et al., 2002). To assess if Arabidopsis GCN5 mediates the heterochromatin phenotypes associated with loss of H3.1K27me1, we created an *atxr5/6 gcn5* triple mutant by crossing a T-DNA insertion allele of *gcn5* (SALK_030913) into the hypomorphic *atxr5/6* mutant background (Jacob et al., 2009). This T-DNA mutant allele of *gcn5* results in the production of a truncated transcript lacking sequence coding for the C-terminus of the GCN5 protein (Supplemental Figure 1A, B). Flow cytometry analyses showed strong suppression of heterochromatin amplification in the triple mutant, as represented by the loss of the characteristic broad peaks corresponding to 8C and 16C endoreduplicated nuclei in *atxr5/6* mutants (Figure 1A and Supplemental Figure 1C). We also observed by microscopy that the heterochromatin decondensation phenotype of *atxr5/6* plants is suppressed in the *atxr5/6 gcn5* triple mutant (Figure 1B, Supplemental Figure 1D). A role for GCN5 in inducing genomic instability in *atxr5/6* was confirmed by observing suppression of heterochromatin amplification using different mutant alleles of *gcn5* (i.e. small indels that change the reading frame of *GCN5* downstream of the start codon in

the first exon) generated by temperature-optimized CRISPR/Cas9 (Supplemental Figure 1A, E, F, G and H) (LeBlanc et al., 2018).

To measure the impact of GCN5 on transcriptional de-repression in *atxr5/6* mutants, we performed RNA-seq analyses and observed widespread suppression of transposable element (TE) reactivation in the *atxr5/6 gcn5* triple mutant compared to *atxr5/6*, although some TEs remained de-repressed compared to Col (Figure 1C and Supplemental Data Set 1). Although *GCN5* has a genome-wide impact on transcription, as shown by the 1781 misregulated genes in *gcn5* single mutants (Figure 1D, Supplemental Data Set 2), none of the known transcriptional suppressors of *atxr5/6* mutants (*SERRATE [SE]*, *AtTHP1*, *AtSAC3B, AtSTUbL2*, *AtMBD9* and *DDM1*) are downregulated in *gcn5* mutants or *atxr5/6 gcn5* triple mutants (Supplemental Figure 1I) (Hale et al., 2016; Ma et al., 2018; Stroud et al., 2012), indicating that suppression of the heterochromatin phenotypes in *atxr5/6 gcn5* is not the result of decreased expression levels of these genes.

GCN5 functions with ADA2b and CHR6 to disrupt heterochromatin in the absence of H3.1K27me1

GCN5 is a member of the multi-subunit SAGA complex, which acts as a transcriptional coactivator in yeast and animals, in part by modifying chromatin (Spedale et al., 2012). Key components of this complex are the proteins GCN5, ADA2, ADA3, and SGF29, which form the histone acetylation module of SAGA (Figure 2A). The Arabidopsis genome contains single genes encoding GCN5 and ADA3 and two genes each encoding ADA2 (*ADA2a* and *ADA2b*) and SGF29 (*SGF29a* and *SGF29b*) (Moraga and Aquea, 2015). *gcn5* and *ada2b* (SALK_019407; (Kornet and Scheres, 2009)) single mutants show pleiotropic phenotypes, which are also shared by the *atxr5/6 gcn5* and *atxr5/6 ada2b* mutants, respectively (Supplemental Figure 2A) (Vlachonasios et al., 2003). To test if ADA2b is also required for inducing the heterochromatin phenotypes of *atxr5/6* mutants, we generated an *atxr5/6 ada2b* triple mutant. The results from flow cytometry experiments show that genomic instability is suppressed in the *atxr5/6 ada2b* triple mutant (Figure 2B and Supplemental Figure 2B). This finding is supported by the altered expression of *BRCA1*, which functions in eukaryotes as a DNA-damage response gene involved in maintaining genome stability (Prakash et al., 2015; Savage and Harkin, 2015). As previously reported, *BRCA1* levels are upregulated in *atxr5/6* (Stroud et al., 2012), and our results show that both *ADA2b* and *GCN5* are required for this

induction (Figure 2C and Supplemental Figure 2C). Like *gcn5*, introducing the *ada2b* mutation into the *atxr5/6* background suppressed transcriptional de-repression of the heterochromatic *TSI* DNA repeat (Figure 2D and Supplemental Figure 2D).

Next, we generated an *atxr5/6 ada3* triple mutant using a T-DNA insertion (SALK_042026C) that prevents expression of a full-length *ADA3* transcript (Supplemental Figure 2E-F), but unlike *atxr5/6 ada2b*, it did not suppress the genome instability phenotype associated with the *atxr5/6* double mutant (Figure 2B). The reported ADA3 protein in Arabidopsis displays low similarity to the ADA3 homologs from yeast and human (26.3% and 16.3%, respectively, compared to >35% similarity for GCN5 and ADA2b (Srivastava et al., 2015)) and might therefore have diverged and not be required for GCN5 and ADA2b to acetylate histones in plants. To further investigate whether another module of SAGA mediates the heterochromatin phenotypes associated with the loss of H3.1K27me1, we created triple mutant combinations between *atxr5/6* and T-DNA mutant alleles of *chr5* or *chr6*. The *chr5* allele (SAIL_504_D01) was characterized in a previous study (Zou et al., 2017), and we performed experiments demonstrating that the *chr6* allele (GK_273E06) contains a T-DNA in an exon that results in a late-flowering phenotype also observed for other mutant alleles of *chr6* (Supplemental Figure 2G-K) (Henderson et al., 2004; Ogas et al., 1997; Ogas et al., 1999). CHR5 and CHR6 are both chromatin-remodeling enzymes that have been proposed to be present in the SAGA complex in plants (Figure 2A). CHR5 is the most closely related plant protein to CHD1-type chromatin remodelers that are part of the SAGA complex in yeast and mammals (Moraga and Aquea, 2015; Srivastava et al., 2015), while CHR6 (also known as CHD3/PICKLE) has been shown to co-purify with SAGA subunits from Arabidopsis tissue (Pfab et al., 2018). Our results show that heterochromatin amplification is suppressed in the *atxr5/6 chr6* triple mutant, but not in *atxr5/6 chr5* (Figure 2E and Supplemental Figure 2G-L), thus suggesting an integral function for CHR6 within SAGA in plants. Like mutations in *GCN5* and *ADA2b*, inactivating *CHR6* in *atxr5/6* mutants suppressed the transcriptional activation of *BRCA1* and *TSI*, and chromatin decondensation (Figure 2F-H and Supplemental Figure 2M). Overall, these results support an essential role for SAGA-mediated histone acetylation in mediating the heterochromatic phenotypes observed in the absence of H3.1K27me1.

GCN5-mediated H3.1K27ac induces the heterochromatin defects associated with loss of H3.1K27me1

The GCN5 homologs in yeast and mammals have been shown to acetylate multiple lysine residues of histone H3 (i.e., K9, K14, K18, K23, K27 and K36) *in vitro*; however, the substrate specificity in the context of different histone H3 variants for GCN5 homologs has been unclear (Cieniewicz et al., 2014; Kuo and Andrews, 2013). In addition, while Arabidopsis GCN5 has been shown to acetylate H3K9 and H3K14 on H3 peptides *in vitro* (Earley et al., 2007), we wanted to examine the role of this protein in acetylation at H3K27 using histone peptides or nucleosomal substrates to better reflect *in vivo* chromatin.

To investigate the substrate specificity of GCN5, we performed *in vitro* histone lysine acetyltransferase (HAT) assays using recombinant nucleosomes containing either plant histone H3.1 or H3.3 variants. We recombinantly expressed and purified an Arabidopsis protein complex composed of GCN5 and ADA2b (Supplemental Figure 3). Our results show that GCN5 has HAT activity at K9, K14, K18, K23, K27, and K36 of histone H3 (Figure 3A). Previous studies have shown that GCN5 is involved in the acetylation of H3K9, H3K14, H3K27, and H3K36 *in vivo* in plants (Chen et al., 2017; Kim et al., 2020; Mahrez et al., 2016), and we validated that it also mediates H3K18ac and H3K23ac by ChIP-qPCR (Supplemental Figure 4A-D). In contrast to ATXR5/6, the enzymatic activity of GCN5 at H3K27 is not regulated by H3 variants, as H3.1 and H3.3 nucleosomes showed equivalent acetylation levels in our HAT assays (Figure 3A). As controls for these results, we used H3.1K27ac and H3.3K27ac peptides to validate that the H3K27ac antibody used did not show preference for H3.1 or H3.3 (Figure 3B), and we validated the specificity of this antibody using H3K27M nucleosomes (Figure 3C). Similar to H3K27, we did not observe any major difference in histone acetyltransferase activity between H3.1 and H3.3 nucleosomes at the other lysine substrates of Arabidopsis GCN5 (Figure 3A). We also confirmed that H3.1K27me1 prevents acetylation by GCN5 at K27 using recombinant nucleosomes mono-methylated at K27 (Figure 3D). To assess if H3.1K27ac mediates the heterochromatin phenotypes present in *atxr5/6* mutants *in vivo*, we introduced a transgene encoding an H3 variant harboring a glutamine residue (Q) instead of K27 (H3K27Q) into wild-type plants. Replacement of lysine with glutamine in histones has been used in *in vivo* chromatin studies to partially mimic the acetylated state of histone lysine residues (Megee et al., 1990; Wang and Hayes, 2008; Zhang et al., 1998).

Our analyses of first-generation transformed (T1) plants showed that expression of H3.1K27Q in wild-type plants is sufficient to induce defects in genome stability, transcriptional activation of the genome instability marker *BRCA1*, and de-repression of the heterochromatic *TSI* repeat (Figure 3E-H). Overall, these results suggest a role for GCN5-mediated H3.1K27ac in inducing the heterochromatic phenotypes associated with the loss of H3.1K27me1 in *atxr5/6* mutants.

H3.1K36 is required to induce genome instability in the absence of H3.1K27me1

Our *in vitro* results suggest that, in addition to K27, other lysine residues on H3.1 could contribute to GCN5-mediated genomic instability in the absence of H3.1K27me1. To assess this hypothesis, we set up a suppressor screen based on *in vivo* replacement of histone H3.1 with the point mutant H3.1S28A. Replacement of serine with alanine on H3.1 variants at position 28 (H3.1S28A) generates H3.1 substrates that cannot be methylated by ATXR5/6 (Figure 4A) (Bergamin et al., 2017). By contrast, H3.1S28A can still be methylated at K27 by plant PRC2-type complexes and acetylated by the GCN5-ADA2b complex, albeit at lower efficiencies (Supplemental Figure 5A-B). We transformed the H3.1S28A transgene into a mutant Arabidopsis background expressing a reduced amount of endogenous histone H3.1 (i.e., *h3.1* quadruple mutant (Jacob et al., 2014)). In T1 plants, we observed phenotypes associated with the loss of H3.1K27me1, including genomic instability (as detected by flow cytometry), increased levels of the genome instability marker gene *BRCA1* (Figure 4B-C), and transcriptional de-repression of the heterochromatic *TSI* DNA repeat (Figure 4D). Attenuated heterochromatic phenotypes in H3.1S28A lines compared to *atxr5/6* mutants are likely due to wild-type H3.1 histone still being present in the *h3.1* quadruple mutant background. These results indicate that expressing H3.1S28A in plants generates phenotypes similar to those of *atxr5/6* mutants due to the loss of H3.1K27me1. We then introduced a series of H3.1S28A expression constructs containing a second mutation (Lys to Arg replacement) at a residue known to be acetylated by GCN5 into the *h3.1* quadruple mutant background and assessed T1 plants for phenotypes associated with the loss of H3.1K27me1. This targeted screen identified H3.1K36 as being essential for inducing genome instability, as flow cytometry analyses demonstrated that H3.1S28A K36R suppresses heterochromatin amplification, while the other targeted mutations do not (Figure 4B). The H3.1S28A K36R replacement line also rescued the increased expression of *BRCA1* (Figure 4C) and the transcriptional de-repression of *TSI* (Figure 4D). Furthermore, expression of the H3.1S28A K36R mutant did not generate a serrated leaf

phenotype, as seen in all the other H3.1S28A lines (Supplemental Figure 6). As mutations at K9, K14, K18, and K23 on the H3.1 variant did not suppress the phenotypes associated with the H3.1S28A mutation, these results indicate a specific role for H3.1K36 in inducing genome instability and transcriptional de-repression in the absence of H3.1K27me1.

GCN5-mediated acetylation of H3.1K36 could be required to induce the heterochromatin defects of *atxr5/6* mutants. One prediction from this model is that increasing histone methylation at H3.1K36 (H3.1K36me) would result in the suppression of the *atxr5/6* mutant phenotypes, as H3.1K36me would antagonize H3.1K36 acetylation by GCN5. To test this notion, we constitutively expressed all five Arabidopsis H3K36 methyltransferase genes (*SDG4*, *SDG7*, *SDG8*, *SDG24*, and *SDG26*) in *atxr5/6* mutants (Baumbusch et al., 2001; Springer et al., 2003). We performed flow cytometry analyses on T1 plants and found that overexpression of *SDG24 (SDG24-OX)* strongly suppresses the heterochromatin amplification phenotype (Figure 4E and Supplemental Figure 7A). We did not observe a similar effect in T1 lines overexpressing *SDG4*, *SDG7*, *SDG8*, or *SDG26* (Supplemental Figure 7B). The ability of *SDG24-OX* to suppress heterochromatin amplification is dependent on SDG24 having a functional methyltransferase (SET) domain, as overexpression of an *SDG24* variant containing a point mutation (Y140N) in a conserved residue essential for SET domain activity did not suppress the phenotype (Figure 4E) (Dillon et al., 2005; Jacob et al., 2010). We performed ChIP-qPCR experiments with *SDG24-OX* plants and detected an increase in H3K36me3 levels at heterochromatic regions (the retrotransposon *Ta3*, *At1g38250,* and *At4g06566*) known to be transcriptionally de-repressed in *atxr5/6* mutants (Figure 4F). Taken together, it is likely that H3K36 methylation opposes some features of the *atrx5/6* phenotypes, potentially by preventing deposition of H3.1K36ac.

Loss of H3.1K27me1 in plants increases H3K27ac and H3K36ac deposition in heterochromatin

Our results support a model in which GCN5 acetylates both H3K27 and H3K36 in the absence of H3.1K27me1 to induce the heterochromatin phenotypes of *atxr5/6* mutants. To assess if H3.1K27me1 depletion leads to an increase in H3K27ac and H3K36ac *in vivo*, we performed ChIP-Rx (ChIP-seq with reference exogenous genome) for H3K27ac and H3K36ac in Col (WT), *atxr5/6*, *gcn5*, and *atxr5/6 gcn5* (Orlando et al., 2014). We found that both histone marks are enriched at the

5' end of protein-coding genes after the transcriptional start site (TSS) in Arabidopsis (Figure 5A) and that this spatial distribution is associated with transcriptional activity, albeit not in a linear relationship (Supplemental Figure 8) (Mahrez et al., 2016; Zhang et al., 2015). Comparative analysis of H3K27ac and H3K36ac in Col and *gcn5* single mutants demonstrated that the loss of GCN5 results in a decrease in H3K27ac and H3K36ac at euchromatic genes (Figure 5A).

Focusing on heterochromatin, which we defined based on previously identified chromatin states in Arabidopsis (Supplemental Data Set 3) (Sequeira-Mendes et al., 2014), we identified 323 regions that were enriched in both H3K27ac and H3K36ac in *atxr5/6* but not in Col plants (Figure 5B-C and Supplemental Data Set 4). H3K27ac and H3K36ac enrichment in heterochromatin was greatly reduced in *atxr5/6 gcn5* triple mutants (Figure 5B-C), suggesting that the higher levels of H3K27ac and H3K36ac in heterochromatic regions of *atxr5/6* are almost completely dependent on GCN5. We next tested if the de-repressed TEs identified in *atxr5/6* by RNA-seq overlap or are in close proximity (± 3kb) to the 323 genomic regions showing increased levels of H3K27ac and H3K36ac in *atxr5/6*. We observed a large overlap between transcriptionally de-repressed genomic regions and regions enriched in H3K27ac and H3K36ac in *atxr5/6* mutants (Figure 5D, Supplemental Data Set 5). The regions shown in Figure 5D likely represent a low estimate of the total overlap between H3K27ac/H3K36ac regions and transposon reactivation due to the inherent lack of sensitivity of ChIP-seq and RNA-seq experiments in backgrounds showing low-level TE de-repression such as *atxr5/6* mutants. For example, we found that a 5-fold increase in sequencing depth (75 versus 15 million reads) in our RNA-seq experiments resulted in a 43% increase in the number of de-repressed TEs identified in *atxr5/6* (446 TEs versus 312 TEs) (Supplemental Data Set 1). To further demonstrate the sensitivity issue associated with low-level de-repression in *atxr5/6*, we performed RT-qPCR on multiple TEs that showed an increase in H3K27ac in *atxr5/6* but were not identified as differently expressed by RNA-seq. For many of these TEs, including *At1g36040* and *At5g29602* (Supplemental Figure 9), we observed higher expression levels in *atxr5/6* compared to wild-type plants, thus confirming the limitations of genome-wide sequencing for detecting low-level TE de-repression in *atxr5/6* mutants. Taken together, these results demonstrate that the loss of H3.1K27me1 in *atxr5/6* mutants leads to GCN5-dependent increases in H3K27ac and H3K36ac in heterochromatin.

H3.1K27me1 regulates the deposition of H3.1K36ac by GCN5

Methylation and acetylation at H3K27 have an antagonistic relationship in the genomes of animals. This relationship is mediated by the interplay between the H3K27 methyltransferase complex PRC2 (H3K27me) and the histone acetyltransferases p300 and CBP, which are responsible for H3K27ac (Pasini et al., 2010; Tie et al., 2009). Our work supports a similar relationship in plants at K27 on H3.1 variants that is mediated by different enzymes, with ATXR5/6-catalyzed H3.1K27me1 preventing the acetylation of H3.1K27 by GCN5. Interactions between post-translational modifications on different histone residues also contribute to chromatin regulation in eukaryotes. One example of this is the inhibition of PRC2 activity towards H3K27 when H3K36 is di- or trimethylated on the same histone (Schmitges et al., 2011; Voigt et al., 2012; Yuan et al., 2011). This suggests that the activity of other chromatin-modifying enzymes may be affected by crosstalk between modified forms of H3K27 and H3K36. To assess if acetylation of H3.1K36 by GCN5 is regulated by H3.1K27me1, we performed *in vitro* HAT assays using recombinant plant nucleosomes containing either unmodified H3.1 or H3.1K27me1. In these assays, we consistently observed a 40% decrease in the levels of acetylation at H3.1K36 on nucleosomes mono-methylated at H3.1K27 compared to unmodified H3.1 (Figure 6A-B). This effect of H3.1K27me1 on Arabidopsis GCN5 activity appears to be specific to H3.1K36, as GCN5-mediated acetylation of H3.1K9 was not affected by mono-methylation at K27. Conversely, we also tested if methylation at H3.1K36 would affect acetylation at K27 by GCN5, but we did not observe any difference in acetylation levels at K27 using K36me0 and K36me3 nucleosomes (Figure 6C). Overall, these results suggest that ATXR5/6-catalyzed H3.1K27me1 in plants interferes with GCN5-mediated acetylation at both H3.1K27 and H3.1K36.

Discussion

Previous work had suggested that transcriptional reactivation of heterochromatic regions is responsible for inducing genomic instability in the absence of H3.1K27me1 in plants (Hale et al., 2016). However, the mechanism by which H3.1K27me1 prevents transcriptional de-repression in heterochromatin was unclear. Our study supports a model where ATXR5/6-mediated H3.1K27me1 serves to prevent a SAGA-like complex that includes GCN5, ADA2b, and CHR6 from acetylating the H3.1 variant and initiating transcriptional de-repression (Figure 6D). K27me1 is the most abundant post-translational modification on H3.1K27 in plants (Johnson et al., 2004), and our

results suggest that it plays a role analogous to the one proposed for PRC2-catalyzed H3K27me2 in animals, which is present on 50-70% of total histone H3 in mouse embryonic stem cells, interferes with H3K27ac deposition, and prevents spurious transcription (Ferrari et al., 2014; Jung et al., 2010; Peters et al., 2003). In animals, p300 and CBP are the main histone acetyltransferases that contribute to H3K27ac in the absence of PRC2-mediated H3K27 methylation (Pasini et al., 2010; Tie et al., 2009). Our results indicate that in plants, GCN5 plays this role. However, transcriptional de-repression is not completely abolished in *gcn5* mutants (Figure 1C), thus suggesting that at least one of the five p300/CBP homologs in Arabidopsis (HAC1/2/4/5/12 (Earley et al., 2007; Li et al., 2014)) may also contribute to higher histone acetylation levels in the absence of H3.1K27me1.

Our work shows that GCN5-catalyzed histone acetylation plays a key role in mediating transcriptional activation in *atxr5/6* mutants. The role of GCN5 as a transcriptional co-activator in other biological systems is well defined, thus supporting a conserved function for GCN5 in all eukaryotes. H3K27ac has been found to be enriched close to the TSS of transcriptionally active protein-coding genes in mammals, maize (*Zea mays*), rice (*Oryza sativa*), and Arabidopsis (Du et al., 2013; Wang et al., 2008; Yan et al., 2019; Zhang et al., 2015), a result that we confirmed for Arabidopsis in our ChIP-Rx experiments. H3K36ac has also been shown in multiple biological systems to co-localize with H3K27ac at the TSS of transcriptionally active regions of the genome (Mahrez et al., 2016; Wang et al., 2008). These observations suggest that TSS-localized H3K27ac and H3K36ac play important roles in mediating transcriptional activity. Precisely mapping the H3K27ac and H3K36ac regions in the heterochromatin of *atxr5/6* mutants in relation to the TSS of de-repressed TEs is challenging, as TSSs are not well defined for TEs. Nevertheless, we did observe H3K27ac and H3K36ac peaks in *atxr5/6* at the 5'ends of annotated TEs (Figure 5C, Supplemental Figure 8), supporting a similar mode of action for H3K27ac/H3K36ac in regulating the transcription of genes and TEs.

Yeast and animal GCN5 have the ability to acetylate multiple lysines (K9, K14, K18, K23, K27, and K36) in the N-terminal tail of histone H3 (Cieniewicz et al., 2014; Kuo and Andrews, 2013). Our *in vitro* and *in vivo* results suggest that the GCN5 homolog in Arabidopsis also has broad substrate specificity. However, the specificity of ATXR5/6 for H3K27 and results from the current study suggest a critical role for K27 over other target sites of GCN5 on H3.1 variants. One

observation supporting a unique role for H3.1K27ac over other acetylated lysines of H3 in Arabidopsis comes from experiments showing that increased levels of cytosolic acetyl-CoA (the essential cofactor for protein acetylation) increase H3 acetylation in plants (Chen et al., 2017). Results from these experiments show that H3K27 is predominantly acetylated over other lysine residues of H3 (i.e. H3K9, H3K14 and H3K18; H3K23 and H3K36 were not assessed in that study) in a manner dependent on GCN5. Higher levels of H3K27ac are observed in genic regions, and this correlates with higher transcriptional levels for genes showing gains in H3K27ac (Chen et al., 2017). Like H3.1K27ac, our *in vitro* and *in vivo* results implicate H3.1K36ac as playing a key role in mediating the heterochromatin phenotypes of *atxr5/6*. However, these results do not rule out the possibility that other acetylated sites (e.g. K9, K14, K18, and K23) on H3.1 also help mediate transcriptional de-repression and genomic instability in plants, for example by acting in a functionally redundant manner. Our *in vitro* histone acetyltransferase assays indicate that deposition of H3K36ac by GCN5 is negatively regulated by H3K27me1, although the molecular mechanism responsible for this crosstalk remains unknown. Previous structural work characterizing a protein complex composed of the histone acetyltransferase (HAT) domain of GCN5 from the unicellular eukaryote *Tetrahymena thermophila* and a phosphorylated histone H3 peptide (aa. 5-23) showed that the HAT domain interacts with the side chain of glutamine 5 (Q5), located nine amino acids upstream of the target lysine (K14) on the H3 peptide (Clements et al., 2003). As H3K27 is similarly located nine amino acids upstream H3K36, this suggests that the HAT domain of GCN5 in Arabidopsis may interact with the side chain of H3K27 to regulate the catalytic activity of GCN5 at H3K36. Structural studies of the HAT domain of Arabidopsis GCN5 will be needed to validate this model.

The catalytic specificity of ATXR5/6 for replication-dependent H3.1 variants, together with the observation that heterochromatin amplification is suppressed when the H3.1 chaperone CAF-1 is mutated, have led to a model in which the H3.1 variant plays a specific role in maintaining genome stability (Jacob et al., 2014). One possible mechanism that could explain the requirement for H3.1 variants to induce the *atxr5/6* mutant phenotypes is that GCN5, like ATXR5/6, specifically modify K27 in H3.1 variants. However, our results show no difference in enzymatic activity for GCN5 on H3.1 vs. H3.3 variants (Figure 3A). Therefore, GCN5 is unlikely to be directly involved in mediating the H3.1 requirement for inducing the *atxr5/6* mutant phenotypes. An alternative

mechanism that could explain the role for H3.1 variants in this process is that downstream chromatin readers that mediate transcriptional de-repression and heterochromatin amplification interact with H3.1K27ac and/or H3.1K36ac, but not H3.3K27ac and/or H3.3K36ac. Another possibility is that transcriptional de-repression mediated through GCN5 is not dependent on H3.1 variants, but heterochromatin amplification is. A previous study showed that expressing an ATXR5/6-resistant H3.1A31T transgene (which partially mimics the N-terminal tail of H3.3 variants) in plants generates low-level transcriptional de-repression in heterochromatin (which is supported by the finding that GCN5 is active on H3.3 variants), but genomic instability in the H3.1A31T lines was not detected (Jacob et al., 2014). Therefore, H3-variant-independent transcriptional de-repression via GCN5 could induce H3.1-dependent genomic instability, or alternatively, these two processes could be uncoupled, although both are regulated by GCN5. Recent work in the yeast *Saccharomyces cerevisiae* demonstrated that passage through S phase of the cell cycle facilitates epigenetic silencing via the insertion of newly synthesized histones. The insertion of newly synthesized histone H3.1 variants in plants during replication could also be a key step in mediating the epigenetic changes that lead to genomic instability in the absence of H3.1K27me1 (Goodnight and Rine, 2020). More work will be needed to fully understand the relationship between H3 variants, transcriptional de-repression, and genomic instability in plants.

Methods

Plant materials

Arabidopsis thaliana plants were grown in Pro-Mix BX Mycorrhizae soil under cool-white fluorescent lights (approximately 100 μmol m^{-2} s^{-1}) in long-day conditions (16 h light/8 h dark). The *atxr5/6* double mutant was described previously (Jacob et al., 2009). *gcn5* (*At3g54610*, SALK_030913), *ada2b* (*At4g16420*, SALK_019407), *ada3* (*At4g29790*, SALK_042026C), *chr5* (*At2g13370*, SAIL_504_D01) and *chr6* (*At2g25170*, GK-273E06) are in the Col-0 genetic background and were obtained from the Arabidopsis Biological Resource Center (Columbus, OH). Temperature-optimized CRISPR/Cas9 was used to generate additional mutant alleles of *GCN5* (in Col-0 and *atxr5/6*) used in this study (LeBlanc et al., 2018). The guide RNA transgenes were segregated away from the mutant alleles. The *h3.1* quadruple mutant was described previously (Jacob et al., 2014). Transgenic plants expressing WT H3.1 (*At5g65360*), H3.1K27Q, H3.1S28A,

H3.1K9R, H3.1S28A K9R, H3.1K14R, H3.1S28A K14R, H3.1K18R, H3.1S28A K18R, H3.1K23R, H3.1S28A K23R, H3.1K36R, and H3.1S28A K36R were made by transforming plants in the *h3.1* quadruple mutant background using the floral dip method (Clough and Bent, 1998). Transgenic plants constitutively expressing (using the 35S promoter) *SDG4*, *SDG7*, *SDG8*, *SDG24*, and *SDG26*) were made by transforming plants in the *atxr5/6* mutant background.

Constructs

Cloning of the catalytic fragment of *ATXR6* (a.a. 25-349) and genes for the plant PRC2 complexes for protein expression and *in vitro* methyltransferase assays was described previously (Jacob et al., 2014; Jacob et al., 2009). The histone H3.1 gene (*At5g65360*) and its promoter (1167 bp upstream of the start codon) were cloned into pENTR/D-TOPO (ThermoFisher Scientific, Waltham, MA) and then sub-cloned using Gateway Technology into the plant binary vectors pB7WG (Karimi et al., 2002). Site-directed mutagenesis to generate the different H3.1 point mutant constructs was performed using a QuikChange II XL Site-Directed Mutagenesis Kit (Agilent Technologies, Santa Clara, CA). PCR products corresponding to the genomic sequences of *SDG4*, *SDG7*, *SGD8*, *SDG24*, and *SDG26* (from start to stop codons) were directly cloned into the pMDC32 vector (Curtis and Grossniklaus, 2003) using the AscI and PacI restriction sites. Site-directed mutagenesis was used to create the Y140N point mutation in *SDG24*. The *ADA2b* coding sequence was cloned into the pETDuet-1 (Millipore, Burlington, MA) vector using the SalI and NotI restriction sites, yielding pETDuet-1-ADA2b. The *GCN5* coding sequence was cloned into the pETDuet-1-*ADA2b* plasmid using the EcoRV and PacI restriction sites, yielding pETDuet-1-*ADA2b*-*GCN5*. The cloning procedure used to make the CRISPR construct targeting *GCN5* in Arabidopsis was performed as described previously (Yan et al., 2015).

Protein expression and purification

Expression and purification of the ATXR6 protein and the plant PRC2 complexes CURLY LEAF and MEDEA were described previously (Jacob et al., 2014; Jacob et al., 2009). Briefly, the GST-tagged ATXR6 protein was expressed in *E. coli* BL21 DE3 cells. Protein expression was induced by adding IPTG to a concentration of 0.1 mM, and induction was allowed to proceed overnight at 20°C. The FLAG-tagged PRC2 complexes CLF and MEA were expressed in SF9 insect cells. To purify the complexes, the SF9 cells were resuspended in lysis buffer (50 mM Tris pH 8.0, 150 mM

NaCl, 1 mM PMSF and 0.1% Triton X-100) and sonicated 10 x 20 seconds on ice. The cell lysate was centrifuged at 20,000 x g for 40 minutes at 4°C, and the complexes were purified with anti-FLAG M2 Affinity Gel (ThermoFisher Scientific). The FLAG fusion complexes were eluted from the columns by competition with 100 µg/ml FLAG peptide (ThermoFisher Scientific) in TBS (50 mM Tris-HCl, 150 mM NaCl, pH 7.4).

For the GCN5-ADA2b protein complex, pETDuet-1-ADA2b-GCN5 was transformed into BL21 (DE3) *E. coli* (Millipore), cultured in LB, and induced to express proteins by adding 1 mM IPTG. The cells were pelleted by centrifugation, resuspended in NPI-10 buffer (50 mM NaH_2PO_4, 300 mM NaCl, 10 mM Imidazole, pH 8), and lysed by sonication. After centrifugation to remove cell debris, Ni-NTA agarose (Qiagen, Hilden, Germany) was added to the supernatant and rotated at 4˚ C for 2 hours. The Ni-NTA agarose was washed 3 times using NPI-20 buffer (50 mM NaH_2PO_4, 300 mM NaCl, 20 mM imidazole, pH 8), and the protein complex was eluted in NPI-250 buffer (50 mM NaH_2PO_4, 300 mM NaCl, 250 mM imidazole, pH 8). The buffer was changed to 1×PBS (137 mM NaCl, 10 mM phosphate, 2.7 mM KCl, pH 7.4) containing 10% glycerol using an Amicon Ultra-0.5 Centrifugal Filter Unit (30 kDa cutoff). The proteins were aliquoted, flash-frozen in liquid nitrogen, and stored at -80˚C.

The protocols to generate the H3K27me1 and H3K36me3 methyl-lysine analog-containing histones and to make the recombinant chromatin used in the *in vitro* histone modification assays (methylation and acetylation) were described previously (Voigt et al., 2012).

Histone lysine methyltransferase (HMT) and acetyltransferase (HAT) assays

The general procedure used to perform the *in vitro* histone modification assays presented in this study were described in detail in a previous publication (Jacob and Voigt, 2018). For the radioactive HMT assays, 0.5 µg of ATXR6, 1.5 µg of MEA or 1.5 µg of CLF (PRC2) complexes were incubated with 1 µg of Histone H3 peptides (GenScript, Piscataway, NJ) and 1.5 µCi of ^{3}H-SAM (Perkin Elmer, Waltham, MA) in a 25 µl reaction. The histone methyltransferase buffer contained 50 mM Tris pH 8.0, 2.5 mM $MgCl_2$ and 4 mM DTT. The methylation reactions were incubated at 22°C for 2 hours. The samples were pipetted onto Whatman P-81 filter paper and dried for 15 minutes. The free ^{3}H-SAM was removed by washing 3 x 30 minutes in 50 mM $NaHCO_3$ pH 9.0.

The filter paper was dried and added to a vial containing Opti-Fluor® O (Perkin Elmer). Radioactivity on the filter papers was determined using a liquid scintillation counter (Perkin Elmer).

For the HAT assays with antibody detection, 1 µg of recombinant nucleosomes and 2 µg of the GCN5-ADA2b complex were incubated in 50 µl histone acetyltransferase (HAT) buffer (1 mM HEPES pH 7.3, 0.02% BSA) containing 50 mM acetyl co-enzyme A (Acetyl-CoA; Sigma) at 23℃ for 3 hours (wild type H3.1, H3.1K27M, and H3.3 nucleosomes) or 5 hours (H3K27me0, H3K27me1, H3K36me0, and H3K36me3 nucleosomes). The reactions were stopped by adding 4X Laemmli Sample Buffer (Bio-Rad) and boiling at 95˚C for 5 minutes. The samples were resolved by 15% SDS-PAGE gel, transferred to PVDF membrane, and immunoblot analysis was performed using anti-H3K9ac (Cell Signaling Technology: Danvers, MA: 9649), anti-H3K14ac (Active Motif, Carlsbad, CA: 39698), anti-H3K18ac (Active Motif: 39588), anti-H3K23ac (Active Motif: 39132), anti-H3K27ac (Active Motif: 39135), anti-H3K36ac (Active Motif: 39379), or anti-H3 antibodies (Abcam: ab1791) and a secondary anti-Rabbit HRP-labeled antibody (Sigma).

For the radioactive HAT assays, 1 µg of peptides and 1 µg of GCN5-ADA2 complex were incubated in 25 µl HAT buffer containing 0.625 µCi ^{3}H-Acetyl-CoA (PerkinElmer) at 23˚C for 2 hours. Reactions were stopped by pipetting onto Whatman P-81 filter paper and dried for 15 minutes. The free ^{3}H-SAM was removed by washing 3 x 30 minutes in 50 mM $NaHCO_3$ pH 9.0. The filter paper was dried, added to a vial containing Opti-Fluor® O (Perkin Elmer) and activity (cpm) was measured using a liquid scintillation counter (Perkin Elmer). No enzyme controls in the HMT and HAT assays consisted of reactions containing buffer, cofactor and chromatin substrate, but no enzyme.

Chromatin Immunoprecipitation

ChIP was performed as described previously (Villar and Kohler, 2010), with some modifications. Briefly, rosette leaves from three-week-old plants were fixed for 15 minutes in 1% formaldehyde. For *SDG24-OX* ChIP experiments, each biological replicate consisted of an independent T1 plant. For ChIP experiments in Supplemental Figure 4 and Figure 5, three plants growing in the same flat were pooled for each biological replicate. After fixation, leaves were flash frozen in liquid nitrogen and ground using a mortar and pestle. Approximately 0.8 g of tissue was added to 10 ml of

extraction buffer 1 (0.4 M sucrose, 10 mM Tris-HCl (pH 8.0), 10 mM $MgCl_2$, 0.1 mM PMSF, 1x protease inhibitors (Roche)) and filtered successively through 70 μm and 40 μm meshes. Samples were centrifuge at 3,000 x g for 20 minutes. The pellets were resuspended in 1 ml of extraction buffer 2 (0.25 M sucrose, 10 mM Tris-HCl (pH 8.0), 10 mM $MgCl_2$, 1% Triton X-100, 0.1 mM PMSF, 1x protease inhibitors) and centrifuged at 12,000 x g for 10 minutes. The pellets were then resuspended in 400 μl of extraction buffer 3 (1.7 M sucrose, 10 mM Tris-HCl (pH 8.0), 0.15% Triton X-100, 0.1 mM PMSF, 1x protease inhibitors). Extraction buffer 3 (400 μl) was added to fresh tubes. The samples were carefully layered over the buffer and centrifuged for 1 hour at 16,000 x g. The pellets were resuspended in nuclei lysis buffer (50 mM Tris-HCl (pH 8.0), 10 mM EDTA, 1% SDS, and 1x protease inhibitors), and chromatin was sheared using a Bioruptor 200 sonicator (20 times on a 30-s ON, 30-s OFF cycle). The supernatants were centrifuged at 16,000 x g for 5 minutes. ChIP dilution buffer (1.1% Triton X-100, 1.2 mM EDTA, 16.7 mM Tris-HCl (pH 8.0), 167 mM NaCl, and 1x protease inhibitors) was added to samples to bring to 10X volume. Antibodies were added to 1 ml of diluted sample and incubated at 4°C overnight (while rotating). 2 μl of Histone H3 antibody (Abcam: ab1791), 2.5 μl of H3K27ac antibody (Active Motif: 39135), 5 μl of H3K36ac antibody (Active Motif: 39379), or 2.5 μl of H3K36me3 (Abcam: ab9050) was used per immunoprecipitation (750 μl of chromatin solution). Immunoprecipitation was performed using protein A magnetic beads (New England BioLabs, Ipswich, MA). The beads were washed twice in each of the following buffers: Low salt wash buffer (150 mM NaCl, 0.1% SDS, 1% Triton X-100, 2 mM EDTA, and 20 mM Tris-HCl (pH 8.0), High salt wash buffer (500 mM NaCl, 0.1% SDS, 1% Triton X-100, 2 mM EDTA, and 20 mM Tris-HCl (pH 8.0)), LiCl wash buffer (0.25 M LiCl, 1% Igepal CA-630, 1% sodium deoxycholate, 1 mM EDTA, and 10 mM Tris-HCl (pH 8.0)) and TE (10 mM Tris-HCl (pH 8.0) and 1 mM EDTA). The beads were resuspended in 500 μl of elution buffer (1% SDS and 0.1 M $NaHCO_3$) and incubated at 65°C for 15 minutes. 20 μl of 5M NaCl was added and samples were incubated at 65°C for 5 hours. 10 μL of 0.5 M EDTA, 20 μL of 1 M Tris-HCl (pH 6.5), and 2 μL of 10 mg/mL proteinase K were added to each sample and incubated for 2 h at 45°C. Immunoprecipitated DNA was purified using a ChIP DNA Clean & Concentrator kit (Zymo Research, Irvine, CA, USA). For the H3K27ac and H3K36ac ChIP experiments, ChIP with exogenous genome (ChIP-Rx) was performed in order to properly normalize the data (Orlando et al., 2014). For each sample, an equal amount of drosophila chromatin (Active Motif #53083) was added prior to chromatin shearing.

DAPI staining of nuclei

Leaves from four-week-old plants were fixed in 3.7% formaldehyde in cold Tris buffer (10 mM Tris-HCl pH 7.5, 10 mM NaEDTA, 100 mM NaCl) for 20 minutes. Formaldehyde solution was removed, and the leaves were washed twice for 10 minutes in Tris buffer. The leaves were then finely chopped with a razor blade in 500 µl LB01 buffer (15 mM Tris-HCl pH 7.5, 2 mM NaEDTA, 0.5 mM spermine-4HCl, 80 mM KCl, 20 mM NaCl, and 0.1% Triton X-100). The lysate was filtered through a 30 µm mesh (Sysmex Partec, Gorlitz, Germany). 5 µl of lysate was added to 10 µl of sorting buffer (100 mM Tris-HCl pH 7.5, 50 mM KCl, 2mM $MgCl_2$, 0.05% Tween-20, and 5% sucrose) and spread onto a coverslip until dried. Cold methanol was added onto each coverslip for 3 minutes, and then rehydrated with TBS-Tx (20 mM Tris pH 7.5, 100 mM NaCl, 0.1% Triton X-100) for 5 minutes. The coverslips were mounted onto slides with Vectashield mounting medium DAPI (Vector Laboratories, Burlingame, CA). Nuclei were imaged under a Nikon Eclipse Ni-E microscope with a 100X CFI PlanApo Lamda objective (Nikon, Minato City, Tokyo, Japan). Digital images were obtained using an Andor Clara camera. Z-series optical sections of each nucleus were obtained at 0.3 µm steps. Images were deconvolved by ImageJ using the deconvolution plugin.

RT-qPCR

Total RNA was extracted from three-week-old leaf tissue using TRIzol (Invitrogen, Carlsbad, CA). The samples were treated with RQ1 RNase-free DNase (Promega, Madison, WI) at 37°C for 30 minutes. SuperScript II Reverse Transcriptase (Invitrogen) was used to produce cDNA from 1 µg of total RNA. Reverse transcription was initiated using oligo dT primers. Quantification of cDNA was done by PCR using a CFX96 Real-Time PCR Detection System (Bio-Rad, Hercules, CA) with KAPA SYBR FAST qPCR Master Mix (2×) Kit (Kapa Biosystems, Wilmington, MA). The cycling conditions were the following: 95°C for 3 minutes; 40 cycles of 95°C for 3 seconds, 60°C for 25 seconds, followed by dissociation curve analysis. Each primer pair was assessed for efficiency of amplification (Supplemental Table 1). Relative quantities were determined by the C_t method (Livak and Schmittgen, 2001). *ACTIN* was used as the normalizer. At least three biological samples were used for each experiment. Three plants growing in the same flat were pooled for each biological replicate.

Flow cytometry

Rosette leaves from three-week-old plants were finely chopped in 0.5 ml Galbraith buffer (45 mM $MgCl_2$, 20 mM MOPS, 30 mM sodium citrate, 0.1% Triton X-100, 40 µg/µl RNase A) using a razor blade. The lysate was filtered through a 30 µm mesh (Sysmex Partec, Gorlitz, Germany). Propidium iodide (Sigma, St. Louis, MO) was added to each sample to a concentration of 20 µg/ml and vortexed for 3 seconds. Each sample was analyzed using a BD FACS LSR Fortessa X20 (Becton Dickinson, Franklin Lakes, NJ). Quantification (nuclei counts and robust CV values) was performed using Flowjo 10.0.6 (Tree Star, Ashland, OR). Each biological replicate consisted of a leaf from one plant.

Next-generation sequencing library preparation

RNA samples were prepared from three-week-old leaf tissue using an RNeasy Plant Mini Kit (Qiagen). Three plants growing in the same flat were pooled for each biological replicate. RNA and ChIP sequencing libraries were prepared at the Yale Center for Genome Analysis (YCGA). RNA samples were quantified and checked for quality using the Agilent 2100 Bioanalyzer Nano RNA Assay. Library preparation was performed using Illumina's TruSeq Stranded Total RNA with Ribo-Zero Plant in which samples were normalized with a total RNA input of 1 µg and library amplification with 8 PCR cycles. ChIP library preparation was performed using a TruSeq Library Prep Kit (Illumina, San Diego, CA). Libraries were validated using the Agilent Bioanalyzer 2100 High sensitivity DNA assay and quantified using a KAPA Library Quantification Kit for Illumina Platforms kit. Sequencing was done on an Illumina NovaSeq 6000 using the S4 XP workflow.

RNA-seq processing and analysis

Two independent biological replicates for Col, *atxr5/6*, *gcn5*, and *atxr5/6 gcn5* were sequenced. Paired-end reads were filtered and trimmed using BBTools (version 38.79) (Bushnell et al., 2017). Reads with quality scores < 20 were removed (Supplemental Table 3). The resulting data sets were aligned against the Arabidopsis genome (TAIR10) using STAR (version 2.7.2a) allowing 2 mismatches (--outFilterMismatchNmax 2) (Dobin et al., 2013). Consistency between biological replicates was confirmed by Pearson correlation using deepTools2 (Supplemental Figure 10) (Ramirez et al., 2016). Protein-coding genes and transposable elements (TE) were defined as

described in the TAIR10 annotation gff3 file. The program featureCounts (version 1.6.4) (Liao et al., 2014) was used to count the paired-end fragments overlapping with the annotated protein-coding genes and TEs. Differential expression analysis of protein-coding genes was performed using DESeq2 version 1.26 (Love et al., 2014) on raw read counts to obtain normalized fold changes (FC) and *Padj*-values for each gene. Genes were considered to be differentially expressed only if they showed a log2FC >1 or log2FC < -1 and a *Padj*-values < 0.05. TPM (transcripts per million) values were calculated for TEs. To define TEs as upregulated in the *atxr5/6* mutant, they must show 2-fold up-regulation compared to Col in both biological replicates and have a value of TPM > 5. The heatmap was drawn with the R program (version 3.6.2) (Team, 2018).

ChIP-seq processing and analysis

Two independent biological replicates for Col, *atxr5/6*, *gcn5*, and *atxr5/6 gcn5* were sequenced. In order to properly compare H3K27ac and H3K36ac levels between each genotype, we performed ChIP-Rx (ChIP with reference exogenous genome) (Orlando et al., 2014) using equal amounts of Drosophila chromatin in each sample as a reference. Paired-end reads were filtered and trimmed using BBTools (Bushnell et al., 2017). Reads with quality scores < 20 were removed (Supplemental Table 3). Data sets were aligned against the combined genomes of *Arabidopsis thaliana* (TAIR10) and *Drosophila melanogaster* (dm6) using bowtie2 (Langmead and Salzberg, 2012) with default parameters. Duplicate reads were removed using Picard toolkit (toolkit., 2019) (MarkesDuplicates with *REMOVE_DUPLICATES=true*). Consistency between biological replicates was confirmed by Pearson correlation using deepTools2 (Supplemental Figure 11) (Ramirez et al., 2016). To calculate the Rx scaling factor of each biological replicate, Drosophila-derived IP read counts were normalized according to the number of input reads. Spike-in normalization was performed as previously described (Nassrallah et al., 2018). We used $\alpha = r/Nd\_IP$ from Orlando *et al*. (2014) to compute the scaling factor α for each replicate, with Nd_IP corresponding to the number of reads (in millions) aligning to the *D. melanogaster* genome in the IP and with $r = 100 * Nd\_i/(Na\_i + Nd\_i)$, where Nd_i and Na_i are the number of input reads (in millions) aligning to the *D. melanogaster* or *A. thaliana* genome, respectively. The Rx factors are presented in Supplemental Table 2. We generated bedgraph files with a bin size of 10 bp using deepTools. The bedgraph files were then scaled by adjusting the number of reads in each bin with the Rx factors and therefore

generating reference-adjusted reads per million (RRPM). H3K27ac and H3K36ac enriched regions were identified by computing the differential between each bin (± 1kb) to define local maxima.

The number of reads corresponding to euchromatic regions was much higher than the ones from heterochromatic regions. To best determine the heterochromatic enrichment of H3K27ac in each genotype of interest, we avoided the noise from the euchromatic reads by first defining heterochromatic regions and extracting the corresponding reads from each genotype. We defined the heterochromatic regions based on chromatin states proposed previously (Sequeira-Mendes et al., 2014). The authors defined four different chromatin states enriched in genes (state 1, state 3, state 6, and state 7), three chromatin states enriched in the distinctive polycomb mark H3K27me3 (state 2, state 4, and state 5), and two types of heterochromatin states (state 8 and state 9). We attributed the value of the state number (1 to 9) for each bin of the Sequeira-Mendes *et al.* annotation, and averaged them on 100 kb windows along the *A. thaliana* genome. Only regions with average chromatin state scores > 7 were defined as heterochromatic regions (Supplemental Data Set 3). We then generated a bam file with the reads corresponding to the defined heterochromatic regions. We identified heterochromatic H3K27ac and H3K36ac-enriched regions by calculating the log2 ratio between H3K27ac or H3K36ac IP and H3 input using the heterochromatin bam file. The enriched regions were defined with the following criteria: log2 (IP/H3) > 0.3. To compare the H3K27ac and H3K36ac enriched regions between Col and our mutant genotypes, we computed log2 (mutant/Col), using the Rx factor normalized bedgraph file. We considered the levels of H3K27ac and H3K36ac to be differential between genotypes when log2 (mutant/Col) > 0.8. These regions needed to be detected in both replicate in order to be considered.

Statistical Analyses

Statistical analysis data are provided in Supplemental Data Set 6.

Primers

All primers used in this study are listed in Supplemental Table 1.

Accession numbers

Sequence data from this article can be found in the GenBank/EMBL libraries under the following accession numbers: ATXR5 (At5g09790), ATXR6 (At5g24330), GCN5 (At3g54610), ADA2b (At4g16420), ADA3 (At4g29790), CHR5, (At2g13370), CHR6 (At2g25170), SDG4 (At4g30860), SDG7 (At2g44150), SDG8 (At1g77300), SDG24 (At3g59960), SDG26 (At1g76710), CLF (At2g23380), MEA (At1g02580), H3.1 (At5g65360), BRCA1 (At4g21070), SE (At2g27100), AtTHP1 (At2g19560), AtSAC3B (At3g06290), AtSTUbL2 (At1g67180), AtMBD9 (At3g01460) and DDM1 (At5g66750).

Sequencing data are available at the Gene Expression Omnibus (GEO) under accession code GSE146126.

Supplemental Data

Supplemental Figure 1. Effect of *GCN5* on genome stability and transcriptional de-repression.

Supplemental Figure 2. Role of SAGA-related proteins in transcriptional de-repression and genome stability.

Supplemental Figure 3. Purification of the GCN5-ADA2b complex.

Supplemental Figure 4. *In vivo* acetylation levels at different lysines of H3 are dependent on *GCN5*.

Supplemental Figure 5. *In vitro* histone modification assays.

Supplemental Figure 6. Growth and developmental phenotypes of T1 plants expressing different H3.1 transgenes.

Supplemental Figure 7. Analyses of the effects of overexpression of H3K36 methyltransferases on genome stability.

Supplemental Figure 8. Average distribution of H3K27ac and H3K36ac over protein-coding genes grouped by their expression levels.

Supplemental Figure 9. Validation of ChIP-seq and RNA-seq analyses.

Supplemental Figure 10. Scatterplots and Pearson correlation coefficients for RNA-seq replicates of Col, *atxr5/6*, *gcn5* and *atxr5/6 gcn5***.**

Supplemental Figure 11. Scatterplots and Pearson correlation coefficients for H3K27ac and H3K36ac ChIP-seq replicates of Col, *atxr5/6*, *gcn5* and *atxr5/6 gcn5*.

Supplemental Table 1. Cloning and PCR primers

Supplemental Table 2. Rx factors for Col, *atxr5/6*, *gcn5* and *atxr5/6 gcn5* replicates.

Supplemental Table 3. Statistics for mapping and coverage of the NGS data.

Supplemental Data Set 1. TEs de-repressed in *atxr5/6*.

Supplemental Data Set 2. Misregulated genes in *atxr5/6*, *gcn5* and *atxr5/6 gcn5*.

Supplemental Data Set 3. Regions of Arabidopsis genome defined as heterochromatin.

Supplemental Data Set 4. Heterochromatic regions enriched in H3K27ac and H3K36ac in *atxr5/6*.

Supplemental Data Set 5. TEs that are de-repressed and overlap with heterochromatic regions enriched in H3K27ac and H3K36ac in *atxr5/6*.

Supplemental Data Set 6. Statistical analysis data.

Acknowledgments

We thank members of our lab for discussions and advice during the course of this work. We want to acknowledge Christopher Bolick and his staff at Yale for help with plant growth and maintenance. We also thank Jean-François Couture (University of Ottawa) for sending the K27M nucleosomes used in this study, and Kenneth Nelson (Yale University) for technical help with flow cytometry. This project was supported by grant #R35GM128661 from the National Institutes of Health to Y.J. B.M. was supported by a Yale University Brown Fellowship. V.J. is supported by the Fonds de Recherche du Québec-Nature et Technologies (FRQNT) [272565]. Work in the Voigt lab is supported by the Wellcome Trust ([104175/Z/14/Z], Sir Henry Dale Fellowship to P.V.) and the European Research Council (ERC) under the European Union's Horizon 2020 research and innovation programme (ERC-STG grant agreement No. 639253). The Wellcome Centre for Cell Biology is supported by core funding from the Wellcome Trust [203149]. We are grateful to the Edinburgh Protein Production Facility (EPPF) for their support. The EPPF was supported by the Wellcome Trust through a Multi-User Equipment grant [101527/Z/13/Z]. The authors declare that they have no competing interests.

Author Contributions

Y.J., J.D., C.L. and A.P. designed the experiments. Y.J. wrote the paper with contributions from J.D., C.L. and A.P. All *in vitro* assays were performed by J.D. C.L. performed the ChIP experiments. A.P. did the bioinformatics analyses of all ChIP-seq experiments. A.P. and V.J. did RNA-seq analyses. Microscopy was done by C.L. Flow cytometry analyses were performed by C.L., B.M, G.V and J.M. RNA extractions and RT-qPCR were done by C.L. and J.D and G.V. Crosses were done by G.V. and B.M. Genotyping and plant transformations were performed by G.V., J.M., C.L., and B.M. G.V. made the CRISPR/Cas9 mutants. K.M.W. and P.V. made the modified and unmodified nucleosomes used in the *in vitro* assays.

References

Baumbusch, L.O., Thorstensen, T., Krauss, V., Fischer, A., Naumann, K., Assalkhou, R., Schulz, I., Reuter, G., and Aalen, R.B. (2001). The Arabidopsis thaliana genome contains at least 29 active genes encoding SET domain proteins that can be assigned to four evolutionarily conserved classes. Nucleic Acids Res 29:4319-4333.

Bergamin, E., Sarvan, S., Malette, J., Eram, M.S., Yeung, S., Mongeon, V., Joshi, M., Brunzelle, J.S., Michaels, S.D., Blais, A., et al. (2017). Molecular basis for the methylation specificity of ATXR5 for histone H3. Nucleic Acids Res 45:6375-6387.

Bushnell, B., Rood, J., and Singer, E. (2017). BBMerge - Accurate paired shotgun read merging via overlap. PLoS One 12:e0185056.

Chen, C., Li, C., Wang, Y., Renaud, J., Tian, G., Kambhampati, S., Saatian, B., Nguyen, V., Hannoufa, A., Marsolais, F., et al. (2017). Cytosolic acetyl-CoA promotes histone acetylation predominantly at H3K27 in Arabidopsis. Nat Plants 3:814-824.

Chen, J.M., Cooper, D.N., Ferec, C., Kehrer-Sawatzki, H., and Patrinos, G.P. (2010). Genomic rearrangements in inherited disease and cancer. Semin Cancer Biol 20:222-233.

Cieniewicz, A.M., Moreland, L., Ringel, A.E., Mackintosh, S.G., Raman, A., Gilbert, T.M., Wolberger, C., Tackett, A.J., and Taverna, S.D. (2014). The bromodomain of Gcn5 regulates site specificity of lysine acetylation on histone H3. Mol Cell Proteomics 13:2896-2910.

Clements, A., Poux, A.N., Lo, W.S., Pillus, L., Berger, S.L., and Marmorstein, R. (2003). Structural basis for histone and phosphohistone binding by the GCN5 histone acetyltransferase. Mol Cell 12:461-473.

Clough, S.J., and Bent, A.F. (1998). Floral dip: a simplified method for Agrobacterium-mediated transformation of Arabidopsis thaliana. Plant J 16:735-743.

Curtis, M.D., and Grossniklaus, U. (2003). A gateway cloning vector set for high-throughput functional analysis of genes in planta. Plant Physiol 133:462-469.

696 Davarinejad, H., Joshi, M., Ait-Hamou, N., Munro, K., and Couture, J.F. (2019). ATXR5/6 Forms
697 Alternative Protein Complexes with PCNA and the Nucleosome Core Particle. J Mol Biol
698 431:1370-1379.
699 Dillon, S.C., Zhang, X., Trievel, R.C., and Cheng, X. (2005). The SET-domain protein superfamily:
700 protein lysine methyltransferases. Genome Biol 6:227.
701 Dobin, A., Davis, C.A., Schlesinger, F., Drenkow, J., Zaleski, C., Jha, S., Batut, P., Chaisson, M.,
702 and Gingeras, T.R. (2013). STAR: ultrafast universal RNA-seq aligner. Bioinformatics
703 29:15-21.
704 Du, Z., Li, H., Wei, Q., Zhao, X., Wang, C., Zhu, Q., Yi, X., Xu, W., Liu, X.S., Jin, W., et al.
705 (2013). Genome-wide analysis of histone modifications: H3K4me2, H3K4me3, H3K9ac,
706 and H3K27ac in Oryza sativa L. Japonica. Mol Plant 6:1463-1472.
707 Earley, K.W., Shook, M.S., Brower-Toland, B., Hicks, L., and Pikaard, C.S. (2007). In vitro
708 specificities of Arabidopsis co-activator histone acetyltransferases: implications for histone
709 hyperacetylation in gene activation. Plant J 52:615-626.
710 Ferrari, K.J., Scelfo, A., Jammula, S., Cuomo, A., Barozzi, I., Stutzer, A., Fischle, W., Bonaldi, T.,
711 and Pasini, D. (2014). Polycomb-dependent H3K27me1 and H3K27me2 regulate active
712 transcription and enhancer fidelity. Mol Cell 53:49-62.
713 Fischle, W., Wang, Y., Jacobs, S.A., Kim, Y., Allis, C.D., and Khorasanizadeh, S. (2003).
714 Molecular basis for the discrimination of repressive methyl-lysine marks in histone H3 by
715 Polycomb and HP1 chromodomains. Genes Dev 17:1870-1881.
716 Goodnight, D., and Rine, J. (2020). S-phase-independent silencing establishment in Saccharomyces
717 cerevisiae. Elife 9.
718 Hale, C.J., Potok, M.E., Lopez, J., Do, T., Liu, A., Gallego-Bartolome, J., Michaels, S.D., and
719 Jacobsen, S.E. (2016). Identification of Multiple Proteins Coupling Transcriptional Gene
720 Silencing to Genome Stability in Arabidopsis thaliana. PLoS Genet 12:e1006092.
721 Hansen, K.H., Bracken, A.P., Pasini, D., Dietrich, N., Gehani, S.S., Monrad, A., Rappsilber, J.,
722 Lerdrup, M., and Helin, K. (2008). A model for transmission of the H3K27me3 epigenetic
723 mark. Nat Cell Biol 10:1291-1300.
724 Henderson, J.T., Li, H.C., Rider, S.D., Mordhorst, A.P., Romero-Severson, J., Cheng, J.C., Robey,
725 J., Sung, Z.R., de Vries, S.C., and Ogas, J. (2004). PICKLE acts throughout the plant to
726 repress expression of embryonic traits and may play a role in gibberellin-dependent
727 responses. Plant Physiol 134:995-1005.
728 Huang, Y., Jiang, L., Liu, B.Y., Tan, C.F., Chen, D.H., Shen, W.H., and Ruan, Y. (2019). Evolution
729 and conservation of polycomb repressive complex 1 core components and putative
730 associated factors in the green lineage. BMC Genomics 20:533.
731 Jacob, Y., Bergamin, E., Donoghue, M.T., Mongeon, V., LeBlanc, C., Voigt, P., Underwood, C.J.,
732 Brunzelle, J.S., Michaels, S.D., Reinberg, D., et al. (2014). Selective methylation of histone
733 H3 variant H3.1 regulates heterochromatin replication. Science 343:1249-1253.
734 Jacob, Y., Feng, S., LeBlanc, C.A., Bernatavichute, Y.V., Stroud, H., Cokus, S., Johnson, L.M.,
735 Pellegrini, M., Jacobsen, S.E., and Michaels, S.D. (2009). ATXR5 and ATXR6 are H3K27
736 monomethyltransferases required for chromatin structure and gene silencing. Nat Struct Mol
737 Biol 16:763-768.
738 Jacob, Y., Stroud, H., Leblanc, C., Feng, S., Zhuo, L., Caro, E., Hassel, C., Gutierrez, C., Michaels,
739 S.D., and Jacobsen, S.E. (2010). Regulation of heterochromatic DNA replication by histone
740 H3 lysine 27 methyltransferases. Nature 466:987-991.

741 Jacob, Y., and Voigt, P. (2018). In Vitro Assays to Measure Histone Methyltransferase Activity
742 Using Different Chromatin Substrates. Methods Mol Biol 1675:345-360.
743 Johnson, L., Mollah, S., Garcia, B.A., Muratore, T.L., Shabanowitz, J., Hunt, D.F., and Jacobsen,
744 S.E. (2004). Mass spectrometry analysis of Arabidopsis histone H3 reveals distinct
745 combinations of post-translational modifications. Nucleic Acids Res 32:6511-6518.
746 Jung, H.R., Pasini, D., Helin, K., and Jensen, O.N. (2010). Quantitative mass spectrometry of
747 histones H3.2 and H3.3 in Suz12-deficient mouse embryonic stem cells reveals distinct,
748 dynamic post-translational modifications at Lys-27 and Lys-36. Mol Cell Proteomics 9:838-
749 850.
750 Karimi, M., Inze, D., and Depicker, A. (2002). GATEWAY vectors for Agrobacterium-mediated
751 plant transformation. Trends Plant Sci 7:193-195.
752 Kim, S., Piquerez, S.J.M., Ramirez-Prado, J.S., Mastorakis, E., Veluchamy, A., Latrasse, D.,
753 Manza-Mianza, D., Brik-Chaouche, R., Huang, Y., Rodriguez-Granados, N.Y., et al. (2020).
754 GCN5 modulates salicylic acid homeostasis by regulating H3K14ac levels at the 5' and 3'
755 ends of its target genes. Nucleic Acids Res 48:5953-5966.
756 Kornet, N., and Scheres, B. (2009). Members of the GCN5 histone acetyltransferase complex
757 regulate PLETHORA-mediated root stem cell niche maintenance and transit amplifying cell
758 proliferation in Arabidopsis. Plant Cell 21:1070-1079.
759 Kuo, M.H., Brownell, J.E., Sobel, R.E., Ranalli, T.A., Cook, R.G., Edmondson, D.G., Roth, S.Y.,
760 and Allis, C.D. (1996). Transcription-linked acetylation by Gcn5p of histones H3 and H4 at
761 specific lysines. Nature 383:269-272.
762 Kuo, Y.M., and Andrews, A.J. (2013). Quantitating the specificity and selectivity of Gcn5-mediated
763 acetylation of histone H3. PLoS One 8:e54896.
764 Langmead, B., and Salzberg, S.L. (2012). Fast gapped-read alignment with Bowtie 2. Nat Methods
765 9:357-359.
766 LeBlanc, C., Zhang, F., Mendez, J., Lozano, Y., Chatpar, K., Irish, V.F., and Jacob, Y. (2018).
767 Increased efficiency of targeted mutagenesis by CRISPR/Cas9 in plants using heat stress.
768 Plant J 93:377-386.
769 Li, C., Xu, J., Li, J., Li, Q., and Yang, H. (2014). Involvement of Arabidopsis HAC family genes in
770 pleiotropic developmental processes. Plant Signal Behav 9:e28173.
771 Liao, Y., Smyth, G.K., and Shi, W. (2014). featureCounts: an efficient general purpose program for
772 assigning sequence reads to genomic features. Bioinformatics 30:923-930.
773 Livak, K.J., and Schmittgen, T.D. (2001). Analysis of relative gene expression data using real-time
774 quantitative PCR and the 2(-Delta Delta C(T)) Method. Methods 25:402-408.
775 Love, M.I., Huber, W., and Anders, S. (2014). Moderated estimation of fold change and dispersion
776 for RNA-seq data with DESeq2. Genome Biol 15:550.
777 Ma, Z., Castillo-Gonzalez, C., Wang, Z., Sun, D., Hu, X., Shen, X., Potok, M.E., and Zhang, X.
778 (2018). Arabidopsis Serrate Coordinates Histone Methyltransferases ATXR5/6 and RNA
779 Processing Factor RDR6 to Regulate Transposon Expression. Dev Cell 45:769-784 e766.
780 Mahrez, W., Arellano, M.S., Moreno-Romero, J., Nakamura, M., Shu, H., Nanni, P., Kohler, C.,
781 Gruissem, W., and Hennig, L. (2016). H3K36ac Is an Evolutionary Conserved Plant Histone
782 Modification That Marks Active Genes. Plant Physiol 170:1566-1577.
783 Margueron, R., Justin, N., Ohno, K., Sharpe, M.L., Son, J., Drury, W.J., 3rd, Voigt, P., Martin, S.R.,
784 Taylor, W.R., De Marco, V., et al. (2009). Role of the polycomb protein EED in the
785 propagation of repressive histone marks. Nature 461:762-767.

786 Megee, P.C., Morgan, B.A., Mittman, B.A., and Smith, M.M. (1990). Genetic analysis of histone
787 H4: essential role of lysines subject to reversible acetylation. Science 247:841-845.
788 Moraga, F., and Aquea, F. (2015). Composition of the SAGA complex in plants and its role in
789 controlling gene expression in response to abiotic stresses. Front Plant Sci 6:865.
790 Musselman, C.A., Lalonde, M.E., Cote, J., and Kutateladze, T.G. (2012). Perceiving the epigenetic
791 landscape through histone readers. Nat Struct Mol Biol 19:1218-1227.
792 Nassrallah, A., Rougee, M., Bourbousse, C., Drevensek, S., Fonseca, S., Iniesto, E., Ait-Mohamed,
793 O., Deton-Cabanillas, A.F., Zabulon, G., Ahmed, I., et al. (2018). DET1-mediated
794 degradation of a SAGA-like deubiquitination module controls H2Bub homeostasis. Elife 7.
795 Ogas, J., Cheng, J.C., Sung, Z.R., and Somerville, C. (1997). Cellular differentiation regulated by
796 gibberellin in the Arabidopsis thaliana pickle mutant. Science 277:91-94.
797 Ogas, J., Kaufmann, S., Henderson, J., and Somerville, C. (1999). PICKLE is a CHD3 chromatin-
798 remodeling factor that regulates the transition from embryonic to vegetative development in
799 Arabidopsis. Proc Natl Acad Sci U S A 96:13839-13844.
800 Orlando, D.A., Chen, M.W., Brown, V.E., Solanki, S., Choi, Y.J., Olson, E.R., Fritz, C.C., Bradner,
801 J.E., and Guenther, M.G. (2014). Quantitative ChIP-Seq normalization reveals global
802 modulation of the epigenome. Cell Rep 9:1163-1170.
803 Pandey, R., Muller, A., Napoli, C.A., Selinger, D.A., Pikaard, C.S., Richards, E.J., Bender, J.,
804 Mount, D.W., and Jorgensen, R.A. (2002). Analysis of histone acetyltransferase and histone
805 deacetylase families of Arabidopsis thaliana suggests functional diversification of chromatin
806 modification among multicellular eukaryotes. Nucleic Acids Res 30:5036-5055.
807 Pasini, D., Malatesta, M., Jung, H.R., Walfridsson, J., Willer, A., Olsson, L., Skotte, J., Wutz, A.,
808 Porse, B., Jensen, O.N., et al. (2010). Characterization of an antagonistic switch between
809 histone H3 lysine 27 methylation and acetylation in the transcriptional regulation of
810 Polycomb group target genes. Nucleic Acids Res 38:4958-4969.
811 Peters, A.H., Kubicek, S., Mechtler, K., O'Sullivan, R.J., Derijck, A.A., Perez-Burgos, L.,
812 Kohlmaier, A., Opravil, S., Tachibana, M., Shinkai, Y., et al. (2003). Partitioning and
813 plasticity of repressive histone methylation states in mammalian chromatin. Mol Cell
814 12:1577-1589.
815 Pfab, A., Bruckmann, A., Nazet, J., Merkl, R., and Grasser, K.D. (2018). The Adaptor Protein
816 ENY2 Is a Component of the Deubiquitination Module of the Arabidopsis SAGA
817 Transcriptional Co-activator Complex but not of the TREX-2 Complex. J Mol Biol
818 430:1479-1494.
819 Prakash, R., Zhang, Y., Feng, W., and Jasin, M. (2015). Homologous recombination and human
820 health: the roles of BRCA1, BRCA2, and associated proteins. Cold Spring Harb Perspect
821 Biol 7:a016600.
822 Ramirez, F., Ryan, D.P., Gruning, B., Bhardwaj, V., Kilpert, F., Richter, A.S., Heyne, S., Dundar,
823 F., and Manke, T. (2016). deepTools2: a next generation web server for deep-sequencing
824 data analysis. Nucleic Acids Res 44:W160-165.
825 Raynaud, C., Sozzani, R., Glab, N., Domenichini, S., Perennes, C., Cella, R., Kondorosi, E., and
826 Bergounioux, C. (2006). Two cell-cycle regulated SET-domain proteins interact with
827 proliferating cell nuclear antigen (PCNA) in Arabidopsis. Plant J 47:395-407.
828 Savage, K.I., and Harkin, D.P. (2015). BRCA1, a 'complex' protein involved in the maintenance of
829 genomic stability. Febs J 282:630-646.

Schmitges, F.W., Prusty, A.B., Faty, M., Stutzer, A., Lingaraju, G.M., Aiwazian, J., Sack, R., Hess, D., Li, L., Zhou, S., et al. (2011). Histone methylation by PRC2 is inhibited by active chromatin marks. Mol Cell 42:330-341.

Sequeira-Mendes, J., Araguez, I., Peiro, R., Mendez-Giraldez, R., Zhang, X., Jacobsen, S.E., Bastolla, U., and Gutierrez, C. (2014). The Functional Topography of the Arabidopsis Genome Is Organized in a Reduced Number of Linear Motifs of Chromatin States. Plant Cell 26:2351-2366.

Spedale, G., Timmers, H.T., and Pijnappel, W.W. (2012). ATAC-king the complexity of SAGA during evolution. Genes Dev 26:527-541.

Springer, N.M., Napoli, C.A., Selinger, D.A., Pandey, R., Cone, K.C., Chandler, V.L., Kaeppler, H.F., and Kaeppler, S.M. (2003). Comparative analysis of SET domain proteins in maize and Arabidopsis reveals multiple duplications preceding the divergence of monocots and dicots. Plant Physiol 132:907-925.

Srivastava, R., Rai, K.M., Pandey, B., Singh, S.P., and Sawant, S.V. (2015). Spt-Ada-Gcn5-Acetyltransferase (SAGA) Complex in Plants: Genome Wide Identification, Evolutionary Conservation and Functional Determination. PLoS One 10:e0134709.

Stroud, H., Hale, C.J., Feng, S., Caro, E., Jacob, Y., Michaels, S.D., and Jacobsen, S.E. (2012). DNA methyltransferases are required to induce heterochromatic re-replication in Arabidopsis. PLoS Genet 8:e1002808.

Suka, N., Suka, Y., Carmen, A.A., Wu, J., and Grunstein, M. (2001). Highly specific antibodies determine histone acetylation site usage in yeast heterochromatin and euchromatin. Mol Cell 8:473-479.

Team, R.C. (2018). R: A language and environment for statistical computing. R Foundation for Statistical Computing, Vienna, Austria.

Tie, F., Banerjee, R., Stratton, C.A., Prasad-Sinha, J., Stepanik, V., Zlobin, A., Diaz, M.O., Scacheri, P.C., and Harte, P.J. (2009). CBP-mediated acetylation of histone H3 lysine 27 antagonizes Drosophila Polycomb silencing. Development 136:3131-3141.

toolkit., B.I.P. (2019). doi:http://broadinstitute.github.io/picard/.

Villar, C.B., and Kohler, C. (2010). Plant chromatin immunoprecipitation. Methods Mol Biol 655:401-411.

Vlachonasios, K.E., Thomashow, M.F., and Triezenberg, S.J. (2003). Disruption mutations of ADA2b and GCN5 transcriptional adaptor genes dramatically affect Arabidopsis growth, development, and gene expression. Plant Cell 15:626-638.

Voigt, P., LeRoy, G., Drury, W.J., 3rd, Zee, B.M., Son, J., Beck, D.B., Young, N.L., Garcia, B.A., and Reinberg, D. (2012). Asymmetrically modified nucleosomes. Cell 151:181-193.

Wang, X., and Hayes, J.J. (2008). Acetylation mimics within individual core histone tail domains indicate distinct roles in regulating the stability of higher-order chromatin structure. Mol Cell Biol 28:227-236.

Wang, Z., Zang, C., Rosenfeld, J.A., Schones, D.E., Barski, A., Cuddapah, S., Cui, K., Roh, T.Y., Peng, W., Zhang, M.Q., et al. (2008). Combinatorial patterns of histone acetylations and methylations in the human genome. Nat Genet 40:897-903.

Weinert, T., Kaochar, S., Jones, H., Paek, A., and Clark, A.J. (2009). The replication fork's five degrees of freedom, their failure and genome rearrangements. Curr Opin Cell Biol 21:778-784.

Xu, C., Bian, C., Yang, W., Galka, M., Ouyang, H., Chen, C., Qiu, W., Liu, H., Jones, A.E., MacKenzie, F., et al. (2010). Binding of different histone marks differentially regulates the

876 activity and specificity of polycomb repressive complex 2 (PRC2). Proc Natl Acad Sci U S
877 A 107:19266-19271.
878 Yan, L., Wei, S., Wu, Y., Hu, R., Li, H., Yang, W., and Xie, Q. (2015). High-Efficiency Genome
879 Editing in Arabidopsis Using YAO Promoter-Driven CRISPR/Cas9 System. Mol Plant
880 8:1820-1823.
881 Yan, W., Chen, D., Schumacher, J., Durantini, D., Engelhorn, J., Chen, M., Carles, C.C., and
882 Kaufmann, K. (2019). Dynamic control of enhancer activity drives stage-specific gene
883 expression during flower morphogenesis. Nat Commun 10:1705.
884 Yuan, W., Xu, M., Huang, C., Liu, N., Chen, S., and Zhu, B. (2011). H3K36 methylation
885 antagonizes PRC2-mediated H3K27 methylation. J Biol Chem 286:7983-7989.
886 Zhang, W., Bone, J.R., Edmondson, D.G., Turner, B.M., and Roth, S.Y. (1998). Essential and
887 redundant functions of histone acetylation revealed by mutation of target lysines and loss of
888 the Gcn5p acetyltransferase. Embo J 17:3155-3167.
889 Zhang, W., Garcia, N., Feng, Y., Zhao, H., and Messing, J. (2015). Genome-wide histone
890 acetylation correlates with active transcription in maize. Genomics 106:214-220.
891 Zou, B., Sun, Q., Zhang, W., Ding, Y., Yang, D.L., Shi, Z., and Hua, J. (2017). The Arabidopsis
892 Chromatin-Remodeling Factor CHR5 Regulates Plant Immune Responses and Nucleosome
893 Occupancy. Plant Cell Physiol 58:2202-2216.

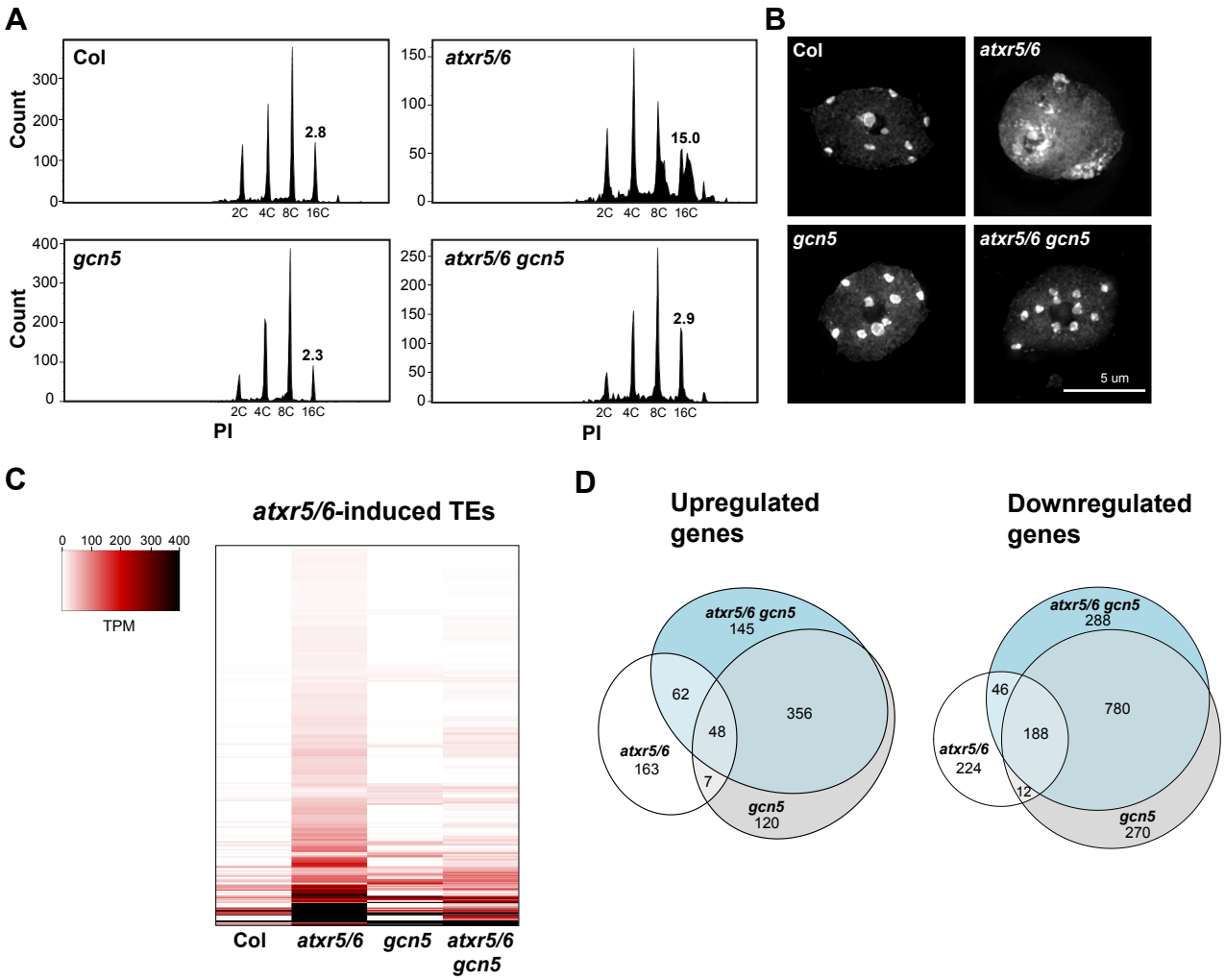

Figure 1. A mutation in *GCN5* suppresses transcriptional de-repression and heterochromatin amplification associated with H3.1K27me1 depletion. (A) Flow cytometry profiles of Col, *atxr5/6*, *gcn5* and *atxr5/6 gcn5* nuclei stained with propidium iodide (PI) with 2000 gated events. The numbers below the peaks indicate ploidy levels of the nuclei. The numbers above the 16C peaks indicate the robust coefficient of variation (CV). (B) Leaf interphase nuclei of Col, *atxr5/6*, *gcn5* and *atxr5/6 gcn5* stained with DAPI. (C) Heat map showing the relative expression levels of 486 *atxr5/6*-induced TEs (Supplemental Table 1) as measured by TPM (transcripts per million) in Col, *atxr5/6*, *gcn5* and *atxr5/6 gcn5*. (D) Euler diagrams showing the number of upregulated and downregulated genes (2-fold change) in *atxr5/6*, *gcn5* and *atxr5/6 gcn5* compared to Col plants (*Padj* < 0.05).

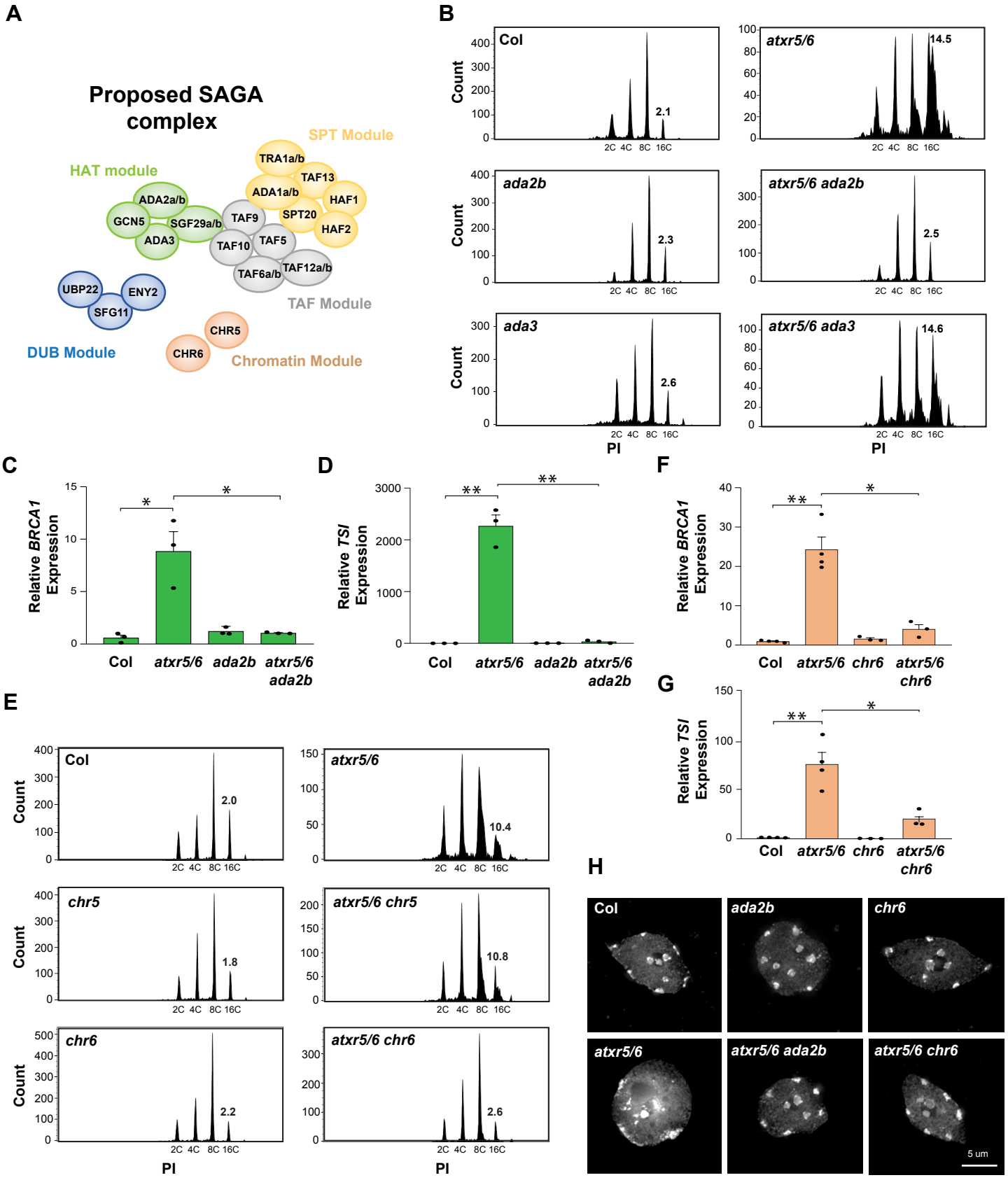

Figure 2. GCN5, ADA2b and CHR6 are required to induce heterochromatic defects in *atxr5/6* mutants. (A) Proposed subunits of the Arabidopsis SAGA complex; adapted from (Moraga and Aquea, 2015). HAT: histone acetylation module; DUB: deubiquitination module; SPT: recruiting module; TAF; coactivator architecture module. (B) Flow cytometry profiles of Col, *atxr5/6*, *ada2b*, *atxr5/6 ada2b*, *ada3*, and *atxr5/6 ada3*. The numbers above the 16C peaks indicate the robust CV. (C and D) RT-qPCR analyses of *BRCA1* (C) and the repetitive element *TSI* (D) in Col, *atxr5/6*, *ada2b* and *atxr5/6 ada2b*. Data represent the mean of three biological replicates and error bars indicate the SEM. Unpaired *t*-test: * $p < 0.05$, ** $p < 0.001$. (E) Flow cytometry profiles of Col, *atxr5/6*, *chr5*, *atxr5/6 chr5*, *chr6*, and *atxr5/6 chr6*. (F and G) RT-qPCR analyses of *BRCA1* (F) and the repetitive element *TSI* (G) in Col, *atxr5/6*, *chr6* and *atxr5/6 chr6*. Data represent the mean of three biological replicates and error bars indicate the standard error of the mean (SEM). Unpaired *t*-test: * $p < 0.05$, ** $p < 0.001$. (H) Leaf interphase nuclei of Col, *atxr5/6*, *ada2b*, *atxr5/6 ada2b, chr6 and atxr5/6 chr6* stained with DAPI.

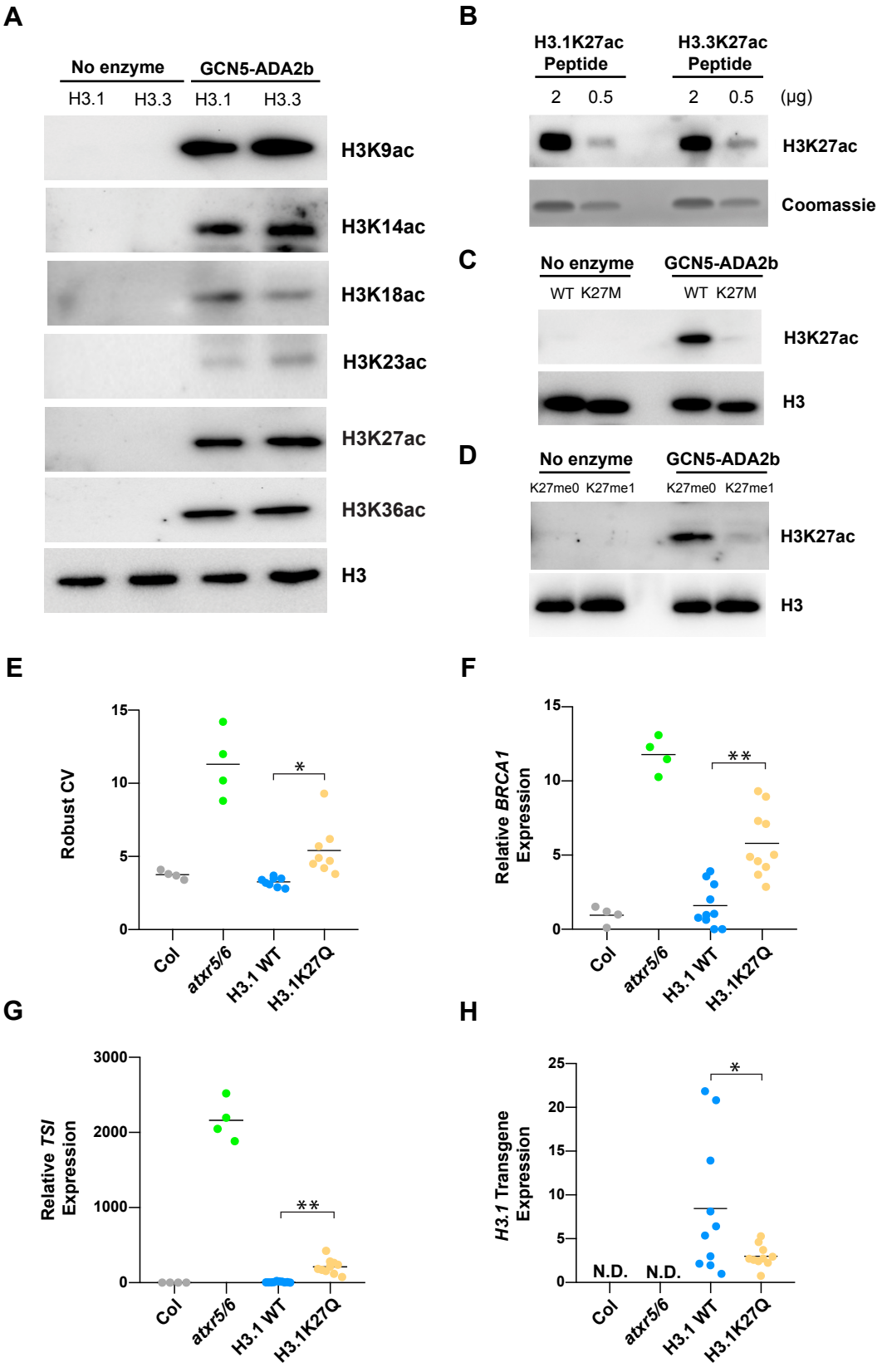

Figure 3. Arabidopsis GCN5 acetylates H3.1K27 and induces the heterochromatic defects associated with *atxr5/6*. (A) *In vitro* HAT assays with the GCN5-ADA2b complex and H3.1 and H3.3 nucleosomes using anti-H3K9ac, anti-H3K14ac, anti-H3K18ac, anti-H3K23ac, anti-H3K27ac, anti-H3K36ac and anti-H3 antibodies for detection. (B) Immunoblot of H3.1K27ac and H3.3K27ac peptides using H3K27ac antibody. (C) *In vitro* HAT assay with the GCN5-ADA2b complex and H3K27M nucleosomes using H3K27ac and H3 antibodes for detection. (D) *In vitro* HAT assays with the GCN5-ADA2b complex and H3K27me0 and H3K27me1 nucleosomes using anti-H3K27ac and anti-H3 antibodies for detection. (E) Robust CV values for 16C nuclei obtained by flow cytometry analysis. For Col and *atxr5/6*, each dot represents an independent biological replicate. For the H3.1 replacement lines, each dot represents one T1 plant. Horizontal bars indicate the mean. Unpaired *t*-test: * $p < 0.01$. (F, G and H) RT-qPCR for the genome stability marker *BRCA1* (F), the heterochromatic transcriptional reactivation marker *TSI* (G) and the *H3.1* transgene (H) in Col, *atxr5/6* and first-generation transformed (T1) plants expressing WT H3.1 or H3.1K27Q. At least eight independent T1 plants were used in the experiments. N.D. = not detected. Unpaired *t*-test: * $p < 0.05$, ** $p < 0.0001$.

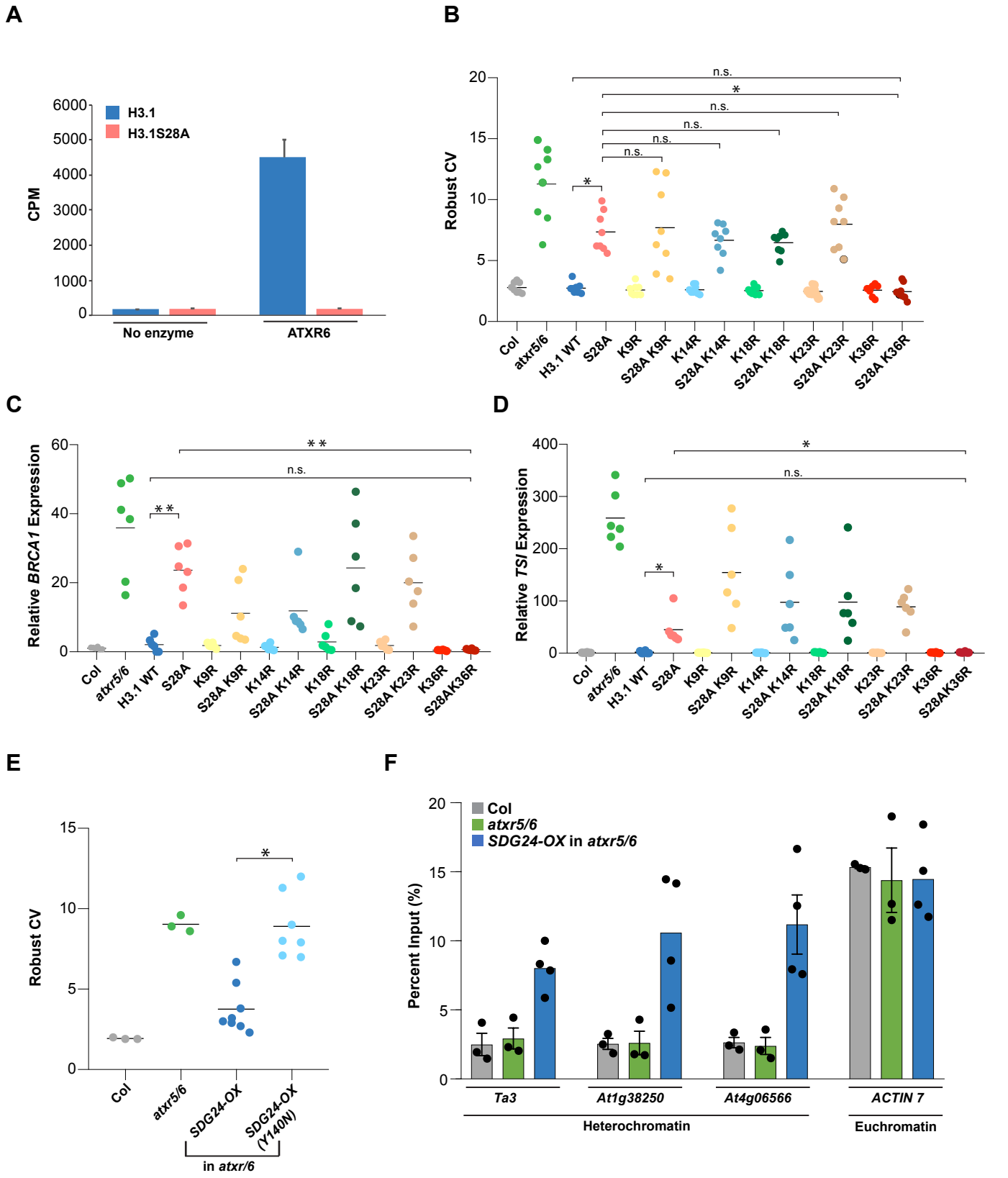

Figure 4. Heterochromatin amplification in the absence of H3.1K27me1 requires H3.1K36 (A) *In vitro* histone lysine methylation assays using H3.1 and H3.1S28A peptide substrates and ATXR6. The average of three experiments and SEM are shown. CPM; counts per minute (B) Robust CV values for 16C nuclei obtained by flow cytometry analysis. For Col and *atxr5/6*, each dot represents an independent biological replicate. For the H3.1 replacement lines, each dot represents one T1 plant. Horizontal bars indicate the mean. Unpaired *t*-test: * $p < 0.00001$ and n.s. = not significantly different. (C and D) RT-qPCR analyses of *BRCA1* (C) and the repetitive element *TSI* (D) in Col, *atxr5/6* and H3.1 replacement lines. For Col and *atxr5/6*, each dot represents an independent biological replicate. For the H3.1 lines, each dot represents one T1 plant. Horizontal bars indicate the mean. Unpaired *t*-test: * $p < 0.01$, ** $p < 0.0001$ and n.s. = not significantly different. (E) Flow cytometry analyses showing robust CV values for 16C nuclei. For the *SDG24-OX* lines, each dot represents one T1 plant. Horizontal bars indicate the mean. Unpaired *t*-test: * $p < 0.0001$. (F) H3K36me3 ChIP-qPCR at *Ta3*, *At1g38250*, *At4g06566* and *ACTIN 7*. For Col and *atxr5/6*, each dot represents an independent biological replicate. For the *SDG24-OX* lines, each dot represents one T1 plant. Bars indicate the mean. Error bars indicate SEM.

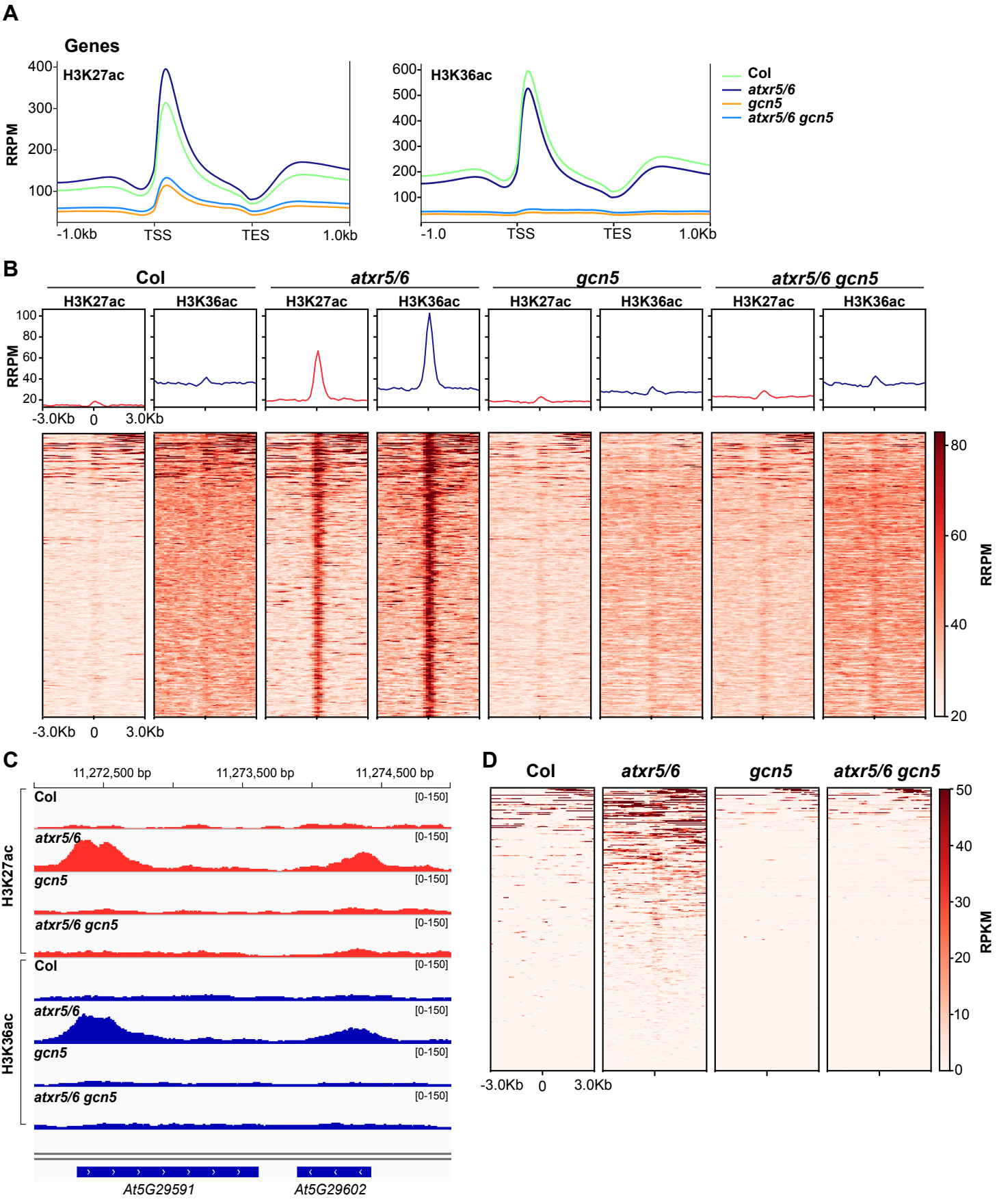

Figure 5. Mutations in *atxr5/6* lead to an increase in H3K27ac and H3K36ac in heterochromatin. (A) Normalized average distribution of H3K27ac and H3K36ac over protein-coding genes for Col, *atxr5/6*, *gcn5* and *atxr5/6 gcn5* in reference-adjusted reads per million (RRPM). TSS, transcription start site; TES, transcription end site. (B) Normalized average distribution and heatmap of H3K27ac and H3K36ac normalized reads surrounding the 323 H3K27ac/H3K36ac-enriched heterochromatic regions identified in *atxr5/6* compared to Col. The regions are sorted based on levels (RRPM) of H3K27ac/H3K36ac enrichment. (C) Genome browser snapshot showing normalized H3K27ac and H3K36ac ChIP-seq data over a region of chromosome 5 that includes TE genes *At5g29591* and *At5g29602*. The *y*-axis unit is RRPM. (D) Heatmap showing the RNA-seq reads mapping to the region ±3 kb around the center of the 323 H3K27ac/H3K36ac peaks as measured by RPKM (reads per kilobase million) in Col, *atxr5/6*, *gcn5* and *atxr5/6 gcn5*. The regions are sorted based on expression level (RPKM).

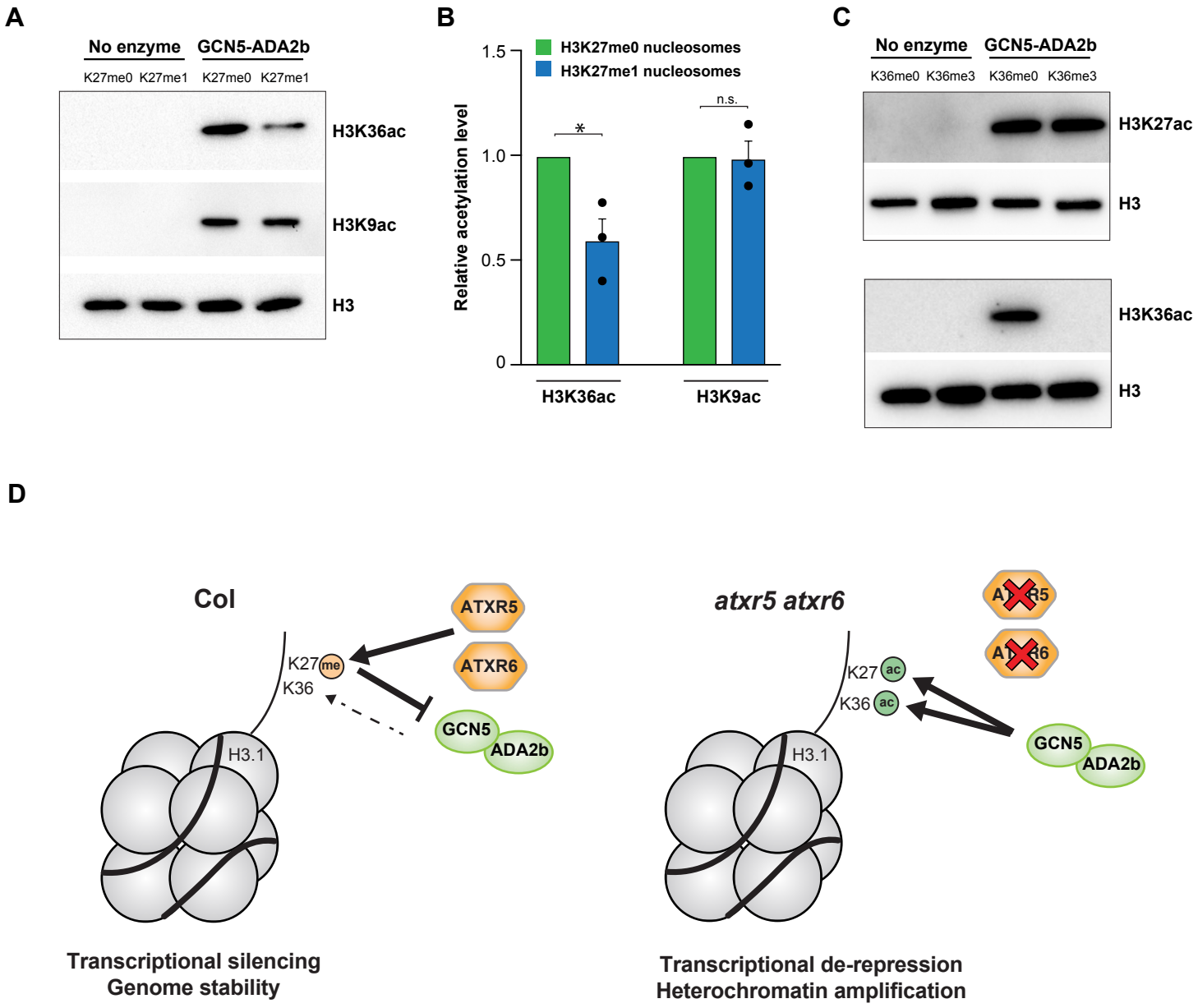

Figure 6. H3K36 acetylation by the GCN5-ADA2b complex is regulated by H3K27me1. (A) *In vitro* HAT assays with the GCN5-ADA2b complex and H3K27me0 and H3K27me1 nucleosomes using H3K36ac, H3K9ac and H3 antibodies for detection. (B) Quantification of HAT assay for three technical replicates using independent preparations of nucleosomes and the GCN5-ADA2b complex. Error bars indicate SEM. Unpaired *t*-test: * $p < 0.05$, and n.s. = not significantly different. (C) *In vitro* HAT assays with the GCN5-ADA2b complex and H3K36me0 and H3K36me3 nucleosomes. Data representative of three technical replicates using independent preparations of the GCN5-ADA2b complex. (D) Model depicting the role of H3.1K27me1 in preventing GCN5-mediated acetylation of H3.1K27 and H3.1K36.